Supporting Information

The Effect of Protein Electrostatic Interactions on Globular Protein-Polymer Block Copolymer Self-Assembly

Christopher N. Lam, Helen Yao, and Bradley D. Olsen*
Department of Chemical Engineering, Massachusetts Institute of Technology, Cambridge, MA 02139

*Corresponding Author

Bradley D. Olsen

TEL) 1-617-715-4548

Email) bdolsen@mit.edu

Sample Preparation and Characterization

Conjugate solutions were concentrated to approximately 100 mg/mL using Millipore Ultra-15 centrifugal filters with a molecular weight cutoff of 10 kDa. Bulk solid samples were then prepared by drop-casting aliquots of the concentrated bioconjugate solution onto Teflon sheets and drying under vacuum overnight at room temperature. For solution studies, the solid material was rehydrated to the desired concentration.

Small-angle X-ray scattering (SAXS) samples were prepared in 1 mm thick washers and sealed with Kapton tape. The bioconjugates with ϕ_{PNIPAM} = 0.52 were measured at the Argonne National Laboratory Advanced Photon Source at Beamline 12-ID-C,D; bioconjugates with ϕ_{PNIPAM} = 0.60 were measured at the Stanford Synchrotron Radiation Lightsource (SLAC), and divalent cation salt studies were performed at Beamline 7.3.3 at the Advanced Light Source. Samples were equilibrated for 10 minutes prior to data collection. SAXS data were corrected for empty cell and dark field scattering, and acquisition times were minimized to prevent beam damage. All observed transitions were reversible with temperature.

Turbidimetry and depolarized light scattering (DPLS)[1,2] were performed on samples loaded into a 1 mm thick Teflon mold and sealed between two quartz disks. A Coherent OBIS LX660 laser was used with wavelength λ = 662 nm (beyond the absorption cutoff of the GFP variants) and continuous wave output power 20 mW. Samples were equilibrated at 10 °C for 20 minutes and then heated at 0.5 °C/min. to 40 °C, allowed to equilibrate for 10 minutes, and then cooled at 0.5 °C/min. to 10 °C. The static depolarized light scattering signal was corrected for transmission and dark field background. For turbidimetry measurements, the same apparatus was used without the rear polarizer to enable measurement of sample transmission. Macrophase separation transitions were defined as the temperatures T_t corresponding to a 10 % reduction in the initial sample transmittance, according to literature methods.[3] Transitions were reproducible upon repeated cycling, and data analysis was performed on the first heating cycle.

For differential scanning calorimetry (DSC) measurements, bioconjugate solution was loaded into a hermetically sealed aluminum pan. Data for five of the six conjugates were acquired using a TA Instruments Discovery differential scanning calorimeter at the Institute for Soldier Nanotechnologies (ISN). Data for the conjugate GFP(-21)-PNIPAM21k were collected using a Texas Instruments Q-10 differential scanning calorimeter in Professor Swager's laboratory in the Department of Chemistry at MIT. The sample was equilibrated at 5 °C for 10 minutes, followed by two cycles of ramping to 45 °C at 5 °C/min., holding isothermally for 2 minutes, cooling at 5 °C/min. to 5 °C, and holding isothermally for 2 minutes. The two measurement cycles overlap, and temperature transition values were extracted from the onset point in the initial heating cycle.

Circular dichroism (CD) spectroscopy was performed using an Aviv model 202 CD spectrometer to measure far UV CD spectroscopy between 190 - 250 nm in a 0.1 cm path length quartz cuvette at a scan rate of 6 nm/min. UV-Vis spectrophotometry was performed using a Varian Cary 50 over the wavelength range 190 - 800 nm in a 1.0 cm path length quartz cuvette at a scan rate of 600 nm/min. GFP(0) was measured in 20 mM Tris-Cl, 250 mM NaCl, pH = 8.0; GFP(-8)

and GFP(-21) were measured in 20 mM Tris-Cl, pH = 8.0; and GFP-PNIPAM conjugates were measured in milliQ water. Measurements were made at T = 10 °C.

Determining PNIPAM Coil Fraction

From published crystallographic data for the superfolder GFP (PDB 2B3P),[4] the crystallized monomeric molecular weights and crystal unit cell parameters and solvent fraction are tabulated as follows:

Parameter	**GFP(-8)**
MW (kg/mol)	29.1444
Formula units *z*	6
Unit cell length *a* (Å)	88.46
Unit cell length *b* (Å)	88.46
Unit cell length *c* (Å)	69.35
Unit cell angle α (°)	90.00
Unit cell angle β (°)	90.00
Unit cell angle γ (°)	120.00
Crystal solvent content ϕ_s (%)	57.92

The protein density is then calculated as follows:

$$\rho_{\text{protein}} = \left(\frac{1}{1-\phi_s} \right) \left(\frac{zMW_{\text{protein}}}{N_A V_{\text{unit cell}}} \right)$$

where N_A is Avogadro's number. The density is calculated to be

$$\rho_{\text{GFP(-8)}} = 1.47 \text{ g cm}^{-3}$$

and this density value is also used for the other two GFP variants, GFP(0) and GFP(-21). Using a density for PNIPAM[5] of 1.05 g cm^{-3}, the PNIPAM coil fraction can then calculated as below:

$$\phi_{\text{PNIPAM}} = \frac{\dfrac{MW_{\text{PNIPAM}}}{\rho_{\text{PNIPAM}}}}{\dfrac{MW_{\text{PNIPAM}}}{\rho_{\text{PNIPAM}}} + \dfrac{MW_{\text{protein}}}{\rho_{\text{protein}}}}$$

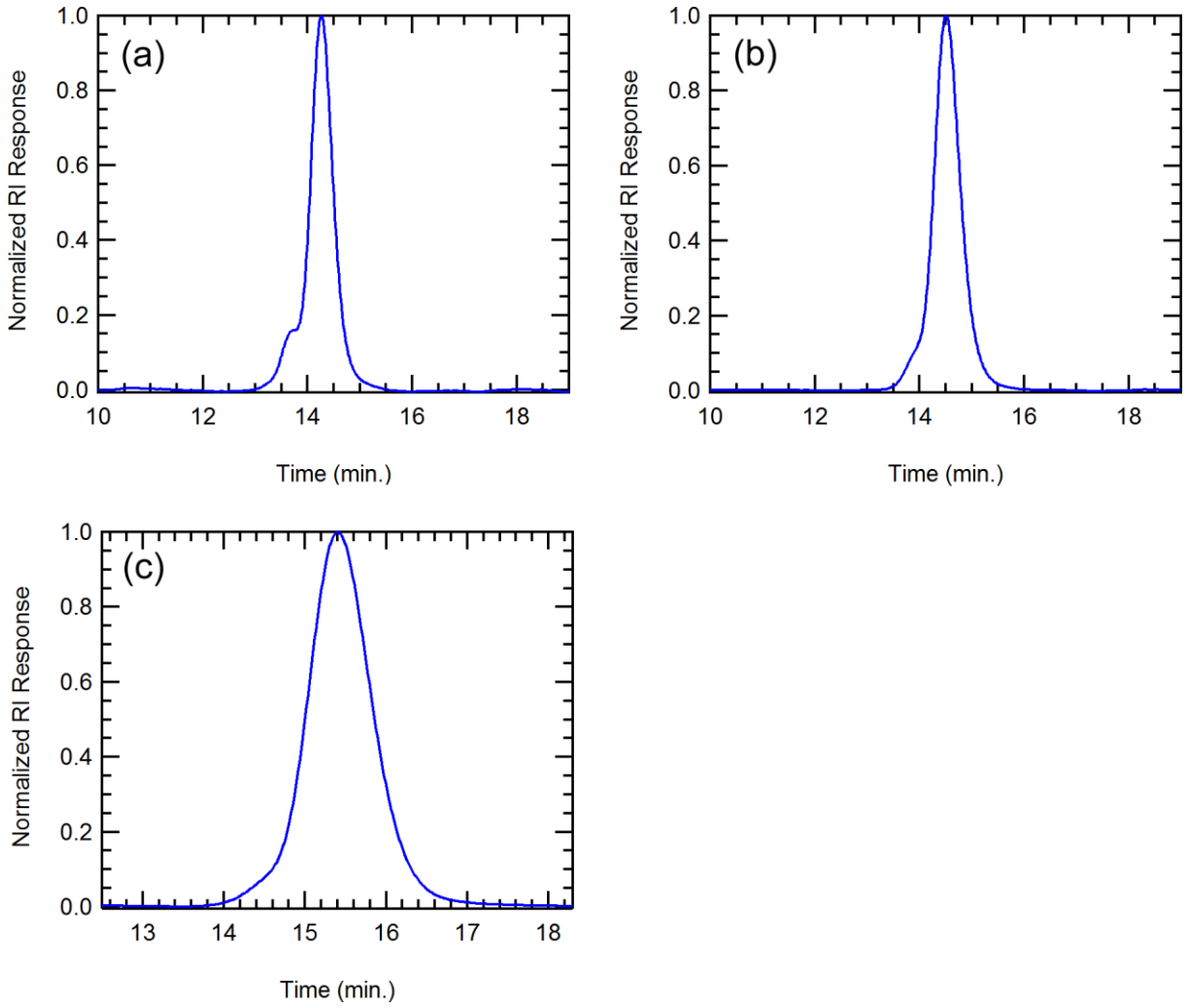

Figure S1. Gel permeation chromatography of (a) PNIPAM30k: M_n = 30,720 g/mol; M_w = 33,580 g/mol; Đ = 1.093, (b) PNIPAM21k: M_n = 21,650 g/mol; M_w = 22,910 g/mol; Đ = 1.058, and (c) PNIPAM4k: M_n = 3840 g/mol; M_w = 4010 g/mol; Đ = 1.043.

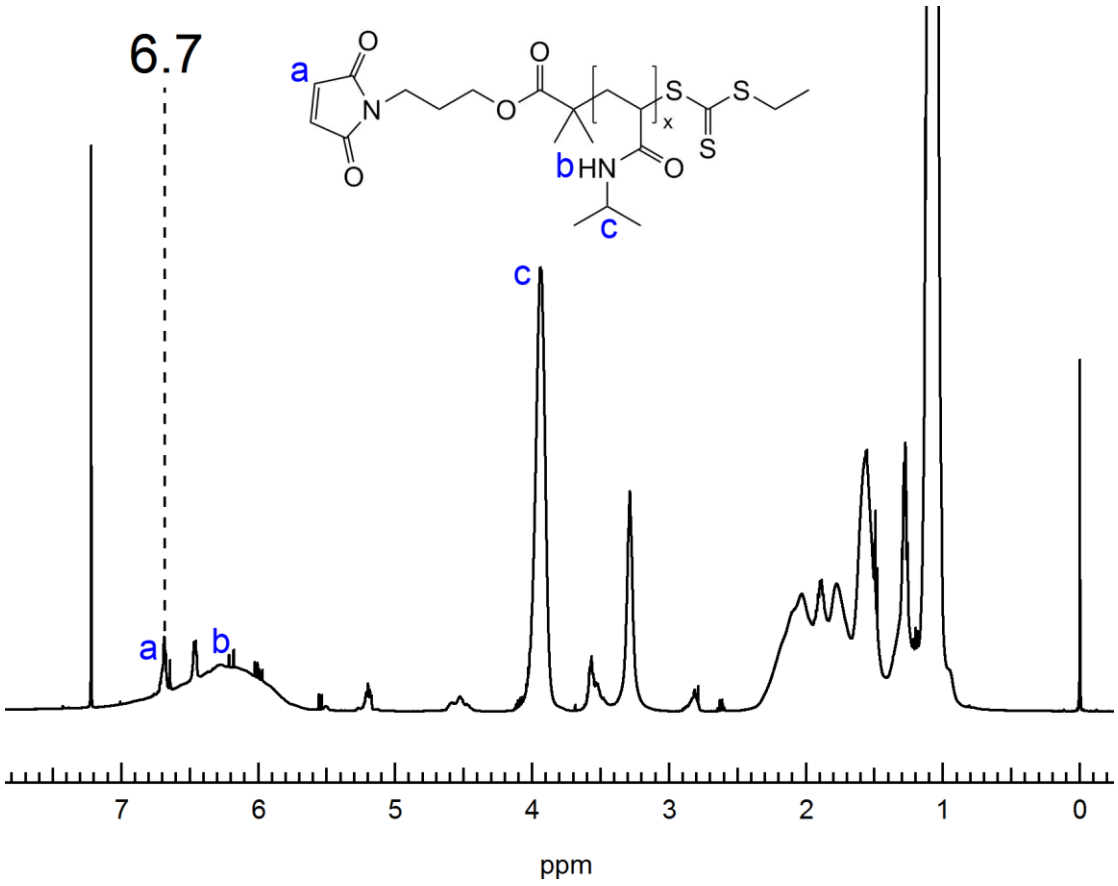

Figure S2. [1]H NMR of maleimide-PNIPAM4k (GPC shown in Figure S1c). A lower molecular weight PNIPAM was measured by NMR to demonstrate that the synthesis yields a maleimide-functionalized PNIPAM. The peak at a chemical shift of 6.7 ppm confirms the presence of the maleimide group. To determine the number of maleimide-functionalized PNIPAM molecules, the areas under the peak corresponding to the maleimide protons (labeled a) and the peak corresponding to the methine proton in the PNIPAM isopropyl group (labeled b) were calculated. Since the maleimide peak was superimposed on the amide peak (labeled c), a Gaussian function was first fit to the amide peak and then subtracted from the maleimide peak to correct the baseline. Once the maleimide peak was corrected, the area under the corrected peak (0.0518, relative integral) was compared to the area under the methine peak (1.1137, relative integral). The ratio between these two peaks was found to be 24.9. Therefore, for every maleimide proton, there are about 25 methine protons. This result was compared to the theoretical result, determined from the GPC results for the 3.8 kDa PNIPAM (Figure S1c). This polymer has 30 monomers, and thus 30 methine protons in the isopropyl group. There are 2 maleimide protons for each polymer. Therefore, if every polymer was end-functionalized, there should be 15 methine protons for every maleimide proton. The NMR result indicates that while not all of the polymer has been end-functionalized, approximately 60% of it does have a maleimide endgroup.

GFP(0) DNA sequence

```
ATGGGACATCACCATCACCATCACGGATCCGCTTGTGAACTGATGGTTTCCAAAGGTGAAGAACTGTTCACCGGTGT
GGTGCCGATCCTGGTTGAGCTGGATGGCGATGTTAACGGTCACAAATTTTCTGTTCGTGGTGAAGGCGAAGGTGACG
CTACTAACGGTAAACTGACTCTGAAATTCATCTGCACCACCGGCAAGCTGCCGGTCCCATGGCCGACCCTGGTAACC
ACCCTGACCTATGGTGTTCAGTGTTTCTCTCGTTATCCGGACCACATGAAACAGCACGATTTCTTTAAGTCCGCGAT
GCCGGAAGGCTACGTTCAGGAACGCACCATCTCTTTCAAAGACGACGGCACTTACAAAACTCGCGCCGAAGTGAAAT
TTGAAGGTGACACCCTGGTGAATCGTATTGAACTGAAGGGTATTGACTTCAAAGAAAAAGGCAACATTCTGGGTCAC
AAGCTGGAGTACAACTTCAACTCTCACAACGTATATATCACCGCAGACAAACGTAAAAATGGCATCAAGGCTAACTT
CAAAATTCGCCACAACGTGAAGGACGGTTCTGTTCAACTGGCTGACCATTACCAGCAAAACACCCCTATTGGTGACG
GCCCGGTTCTGCTGCCGCGTAACCATTATCTGTCCACTCAGTCTGCACTGTCCAAAGACCCAAAAGAAAAACGTGAC
CACATGGTGCTGCTGGAATTTGTGACCGCGGCGGGTATTACCCATGGTATGGACGAGCTGTACAAATAA
```

GFP(0) amino acid sequence

```
MGHHHHHHGSACELMVSKGEELFTGVVPILVELDGDVNGHKFSVRGEGEGDATNGKLTLKFICTTGKLPVPWPTLVT
TLTYGVQCFSRYPDHMKQHDFFKSAMPEGYVQERTISFKDDGTYKTRAEVKFEGDTLVNRIELKGIDFKEKGNILGH
KLEYNFNSHNVYITADKRKNGIKANFKIRHNVKDGSVQLADHYQQNTPIGDGPVLLPRNHYLSTQSALSKDPKEKRD
HMVLLEFVTAAGITHGMDELYK
```

Figure S3. DNA and amino acid sequences of GFP(0).

GFP(-8) DNA sequence

```
ATGGGACATCACCATCACCATCACGGATCCGCCTGCGAACTGATGGTATCTAAAGGTGAGGAACTGTTCACTGGCGT
TGTTCCGATCCTGGTGGAGCTGGATGGCGACGTGAATGGCCACAAATTCAGCGTGCGTGGCGAAGGCGAGGGCGATG
CTACCAACGGTAAACTGACCCTGAAATTCATCTGTACCACTGGTAAACTGCCGGTCCCATGGCCGACCCTGGTGACC
ACTCTGACCTACGGTGTTCAGTGCTTTTCTCGTTACCCGGATCATATGAAACAACATGATTTCTTCAAATCCGCTAT
GCCGGAGGGTTACGTGCAGGAACGTACGATTTCTTTTAAAGATGACGGCACTTATAAAACTCGTGCCGAAGTTAAAT
TTGAGGGCGACACCCTGGTGAACCGTATTGAACTGAAAGGTATCGACTTCAAAGAGGATGGCAACATCCTGGGTCAT
AAACTGGAATATAACTTCAACTCTCACAACGTTTATATCACCGCTGACAAACAGAAAAACGGCATTAAAGCGAATTT
TAAAATCCGTCATAACGTTGAAGACGGTTCTGTTCAGCTGGCAGACCATTATCAGCAAAACACCCCGATCGGTGACG
GCCCTGTTCTGCTGCCGGACAACCATTACCTGTCTACGCAGAGCGCGCTGTCTAAAGACCCGAACGAGAAACGTGAC
CATATGGTTCTGCTGGAATTTGTCACCGCGGCGGGCATTACCCATGGCATGGACGAACTGTATAAGTAA
```

GFP(-8) amino acid sequence

```
MGHHHHHHGSACELMVSKGEELFTGVVPILVELDGDVNGHKFSVRGEGEGDATNGKLTLKFICTTGKLPVPWPTLVT
TLTYGVQCFSRYPDHMKQHDFFKSAMPEGYVQERTISFKDDGTYKTRAEVKFEGDTLVNRIELKGIDFKEDGNILGH
KLEYNFNSHNVYITADKQKNGIKANFKIRHNVEDGSVQLADHYQQNTPIGDGPVLLPDNHYLSTQSALSKDPNEKRD
HMVLLEFVTAAGITHGMDELYK
```

Figure S4. DNA and amino acid sequences of GFP(-8).

GFP(-21) DNA sequence

ATGGGACATCACCATCACCATCACGGATCCGCATGCGAACTGATGGTATCTAAAGGCGAAGAACTGTTTACCGGTGT
AGTGCCGATCCTGGTAGAACTGGACGGTGACGTAAACGGTCATGAGTTTTCTGTGCGTGGCGAAGGTGAAGGTGATG
CTACCGAAGGCGAGCTGACTCTGAAATTTATTTGCACCACCGGTAAACTGCCGGTTCCGTGGCCAACGCTGGTTACC
ACTCTGACGTATGGTGTACAGTGCTTTTCCCGCTACCCAGACCACATGAAACAACACGACTTCTTCAAGTCTGCCAT
GCCGGAAGGCTACGTGCAGGAACGTACGATCAGCTTCAAGGATGATGGTACTTACAAAACTCGCGCAGAAGTGAAAT
TCGAAGGCGACACTCTGGTTAACCGCATCGAACTGAAGGGTATCGACTTTAAAGAAGACGGTAACATCCTGGGTCAC
AAACTGGAATATAACTTCAACTCTCACGACGTCTACATCACCGCGGACAAACAGGAAAACGGCATCAAAGCGGAGTT
CGAAATCCGTCACAACGTTGAAGACGGTAGCGTTCAGCTGGCCGATCACTATCAGCAGAATACTCCTATCGGTGATG
GCCCGGTACTGCTGCCGGACGACCACTACCTGTCCACTGAGTCTGCCCTGTCCAAAGATCCGAACGAAAAACGTGAC
CATATGGTGCTGCTGGAATTTGTAACCGCCGCTGGTATCACCCACGGTATGGATGAGCTGTATAAGTAA

GFP(-21) amino acid sequence

MGHHHHHHGSACELMVSKGEELFTGVVPILVELDGDVNGHEFSVRGEGEGDATEGELTLKFICTTGKLPVPWPTLVT
TLTYGVQCFSRYPDHMKQHDFFKSAMPEGYVQERTISFKDDGTYKTRAEVKFEGDTLVNRIELKGIDFKEDGNILGH
KLEYNFNSHDVYITADKQENGIKAEFEIRHNVEDGSVQLADHYQQNTPIGDGPVLLPDDHYLSTESALSKDPNEKRD
HMVLLEFVTAAGITHGMDELYK

Figure S5. DNA and amino acid sequences of GFP(-21).

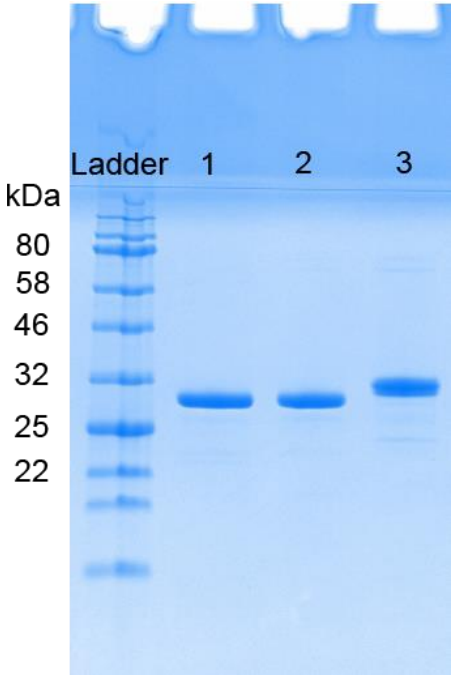

Figure S6. SDS-PAGE of GFP variants. Lanes 1-3 represent GFP(0), GFP(-8), and GFP(-21), respectively.

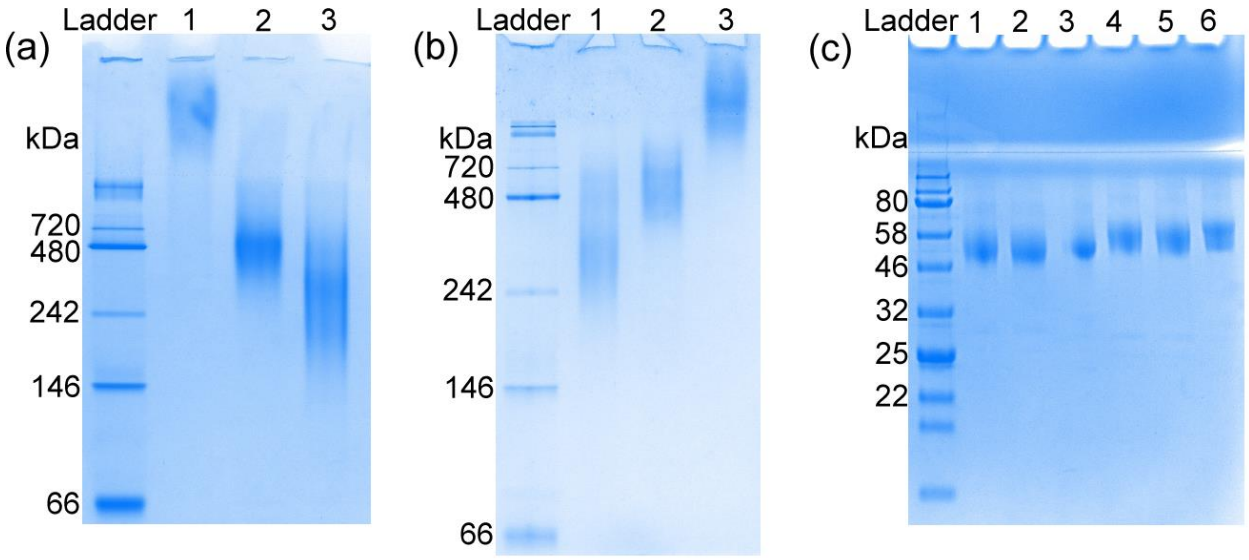

Figure S7. Native PAGE of GFP conjugated to (a) PNIPAM21k and (b) PNIPAM30k. In (a), lanes 1-3 represent GFP(0)PNIPAM21k, GFP(-8)PNIPAM21k, and GFP(-21)PNIPAM21k, respectively. In (b), lanes 1-3 represent GFP(-21)PNIPAM30k, GFP(-8)PNIPAM30k, and GFP(0)PNIPAM30k, respectively. In native PAGE, conjugates of the neutral variant, GFP(0), do not migrate toward the positive electrode and are observed to remain in the stacking gel. Native PAGE shows undetectable levels of impurity, suggesting that the bioconjugates are > 98% pure. (c) SDS-PAGE of bioconjugates. Lanes 1-6 represent GFP(0)PNIPAM21k, GFP(-8)PNIPAM21k, GFP(-21)PNIPAM21k, GFP(0)PNIPAM30k, GFP(-8)PNIPAM30k, and GFP(-21)PNIPAM30k, respectively.

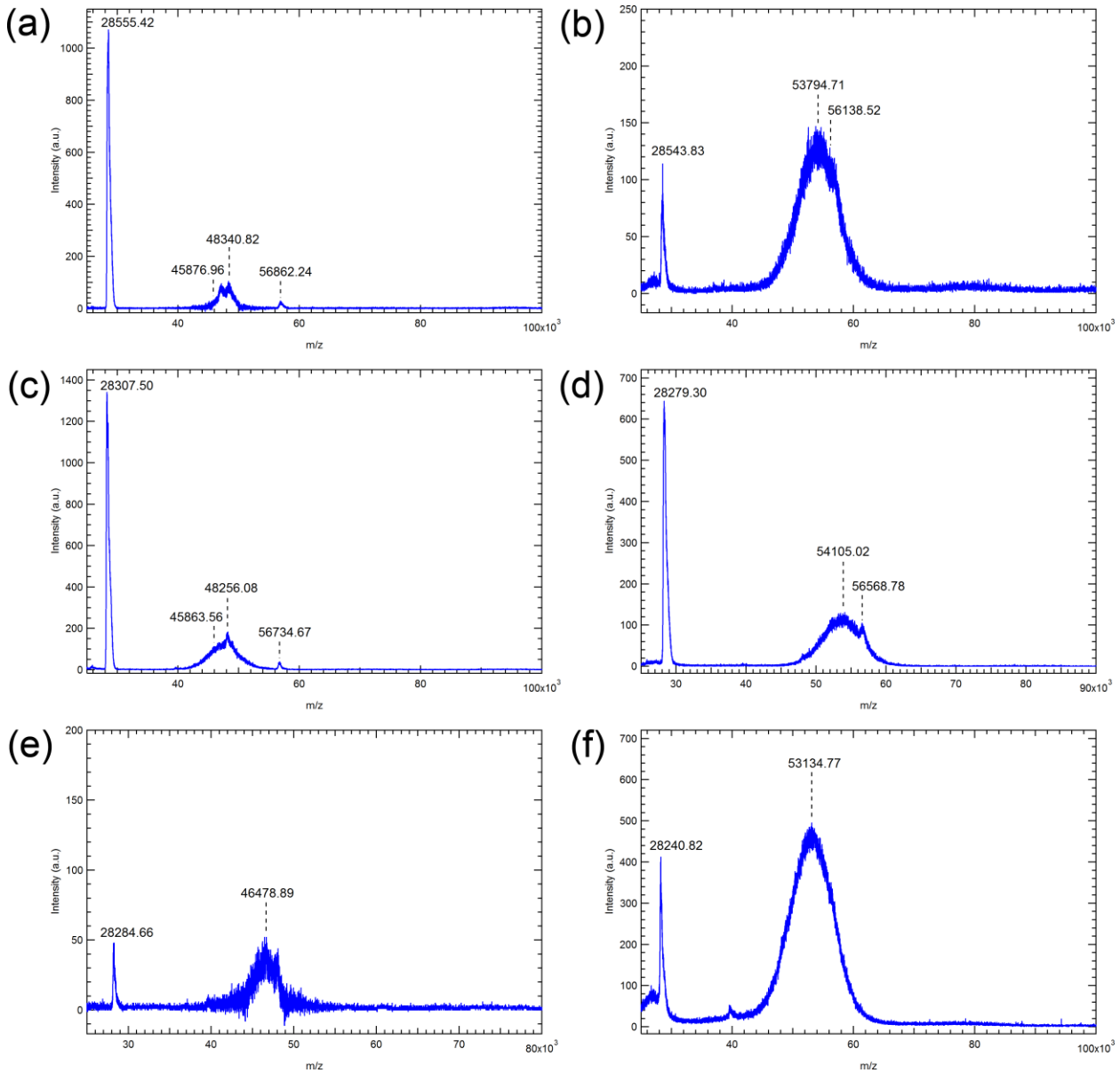

Figure S8. MALDI-TOF mass spectra of GFP-PNIPAM bioconjugates: (a) GFP(0)-PNIPAM21k, (b) GFP(0)-PNIPAM30k, (c) GFP(-8)-PNIPAM21k, (d) GFP(-8)-PNIPAM30k, (e) GFP(-21)-PNIPAM21k, and (f) GFP(-21)-PNIPAM30k.

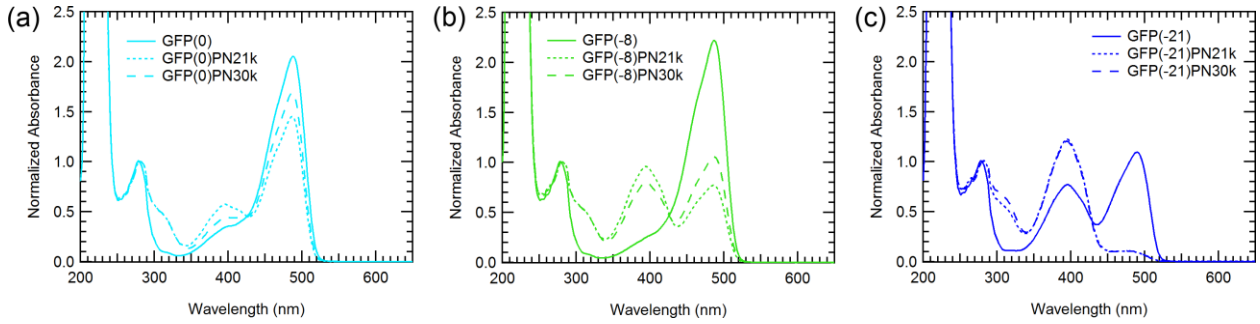

Figure S9. UV-Vis absorption spectra for GFP variants and conjugates to PNIPAM21k and PNIPAM30k for (a) GFP(0), (b) GFP(-8), and (c) GFP(-21). The three different GFP variants have different ratios of absorbance at 395 nm and 488 nm, which correspond to protonated and deprotonated tyrosyl hydroxyl groups, respectively.[6] The different electrostatic properties of the GFP variants is observed to affect the relative ratio of absorbance at 395 and 488 nm. The hydroxyl group is part of a network of hydrogen bonds that is also observed to be perturbed upon conjugation. Similar UV-Vis spectra to those of GFP(-8)-PNIPAM has been observed in previously studied EGFP-PNIPAM conjugates.[7]

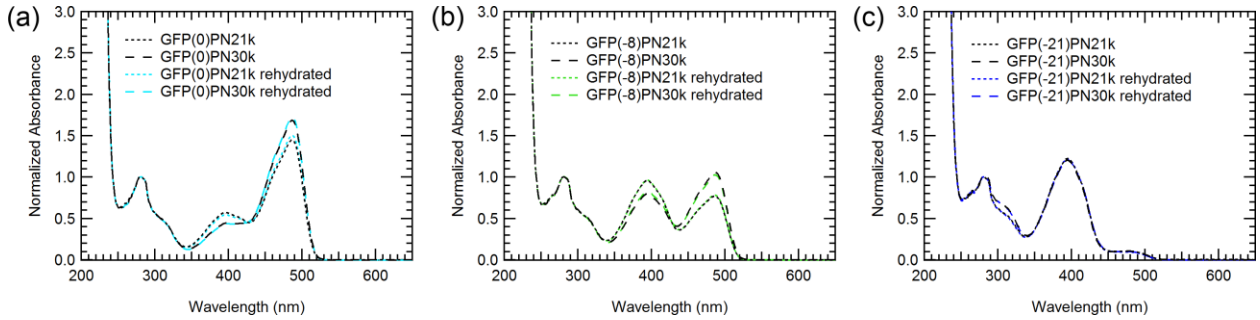

Figure S10. UV-Vis absorption spectra for GFP variants and conjugates to PNIPAM21k and PNIPAM30k after rehydration of solid conjugate pellets for (a) GFP(0), (b) GFP(-8), and (c) GFP(-21), showing minimal change in protein function after self-assembly and rehydration.

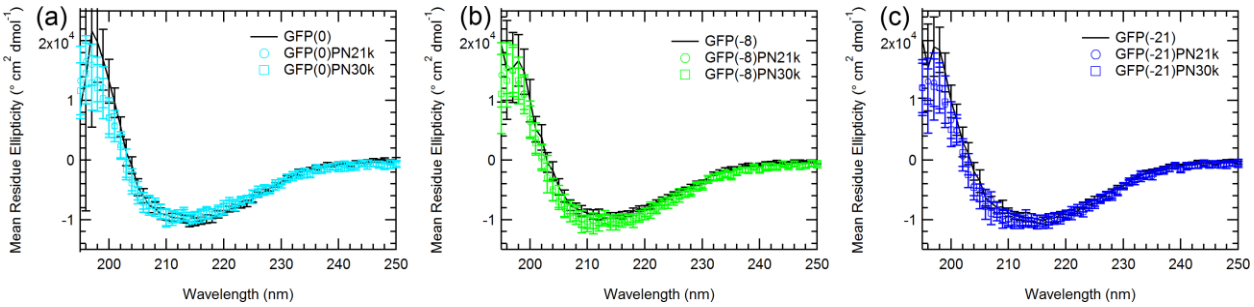

Figure S11. Circular dichroism spectroscopy of GFP variants and conjugates to PNIPAM21k and PNIPAM30k for (a) GFP(0), (b) GFP(-8), and (c) GFP(-21) confirm that the secondary structure is preserved in the conjugates. GFP(0) was measured in 20 mM Tris-Cl, 250 mM NaCl, pH = 8.0, and GFP(-8) and GFP(-21) were measured in 20 mM Tris-Cl, pH = 8.0. Conjugates were measured in milliQ water. Measurements were performed at T = 10 °C.

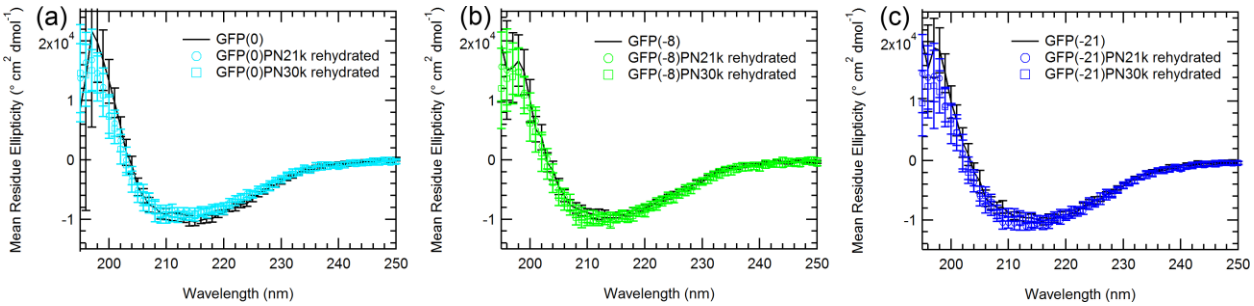

Figure S12. Circular dichroism spectroscopy of GFP variants and conjugates to PNIPAM21k and PNIPAM30k after rehydration of solid conjugate pellets for (a) GFP(0), (b) GFP(-8), and (c) GFP(-21) confirm minimal change in secondary structure after self-assembly and rehydration. GFP(0) was measured in 20 mM Tris-Cl, 250 mM NaCl, pH = 8.0, and GFP(-8) and GFP(-21) were measured in 20 mM Tris-Cl, pH = 8.0. Conjugates were measured in milliQ water. Measurements were performed at T = 10 °C.

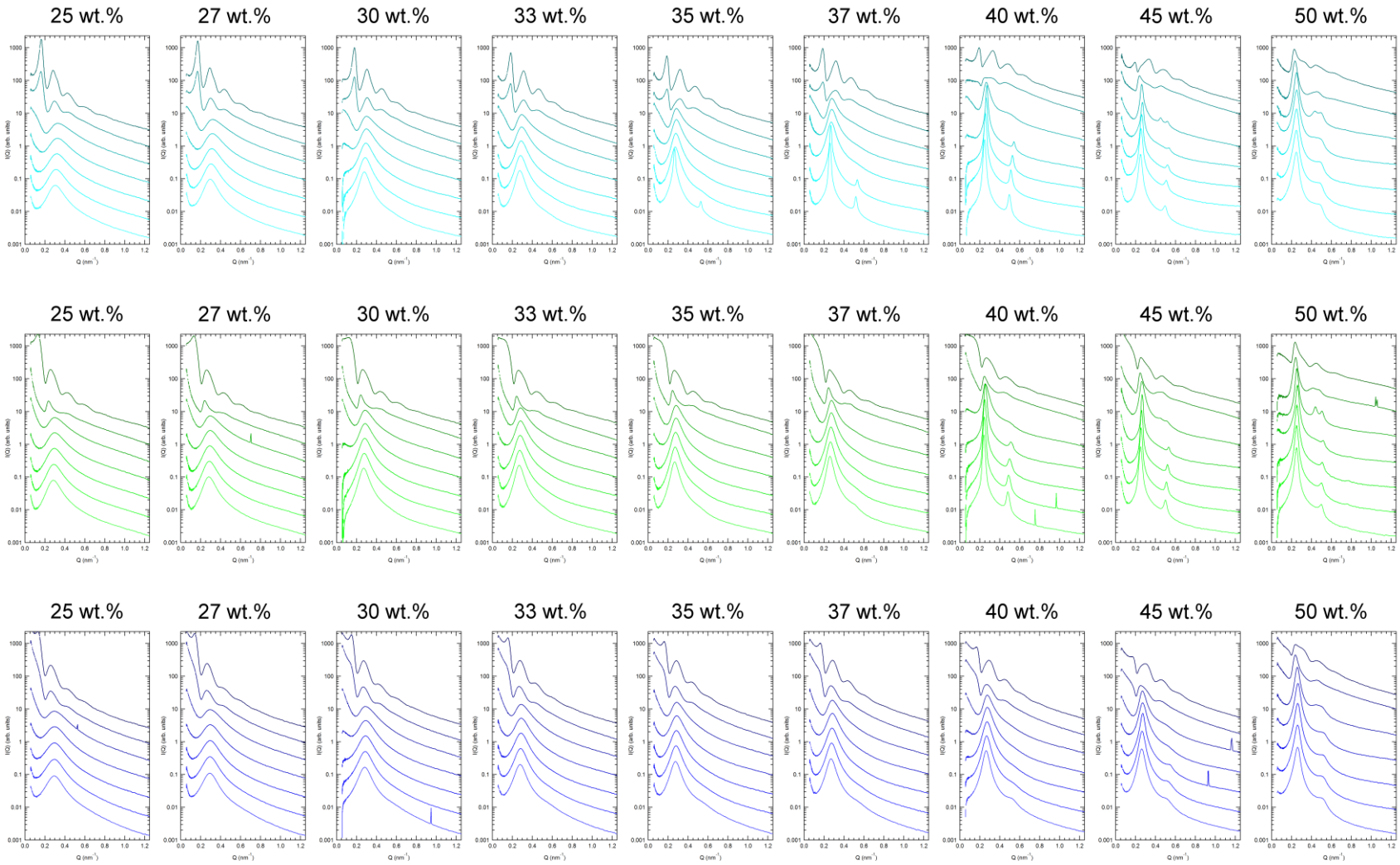

Figure S13. Radially averaged SAXS patterns for (top) GFP(0)-PNIPAM21k, (middle) GFP(-8)-PNIPAM21k, and (bottom) (GFP(-21)-PNIPAM21k. The curves are offset vertically for clarity. The seven curves in each plot increase in temperature upward from 10 to 40 °C in 5 °C intervals.

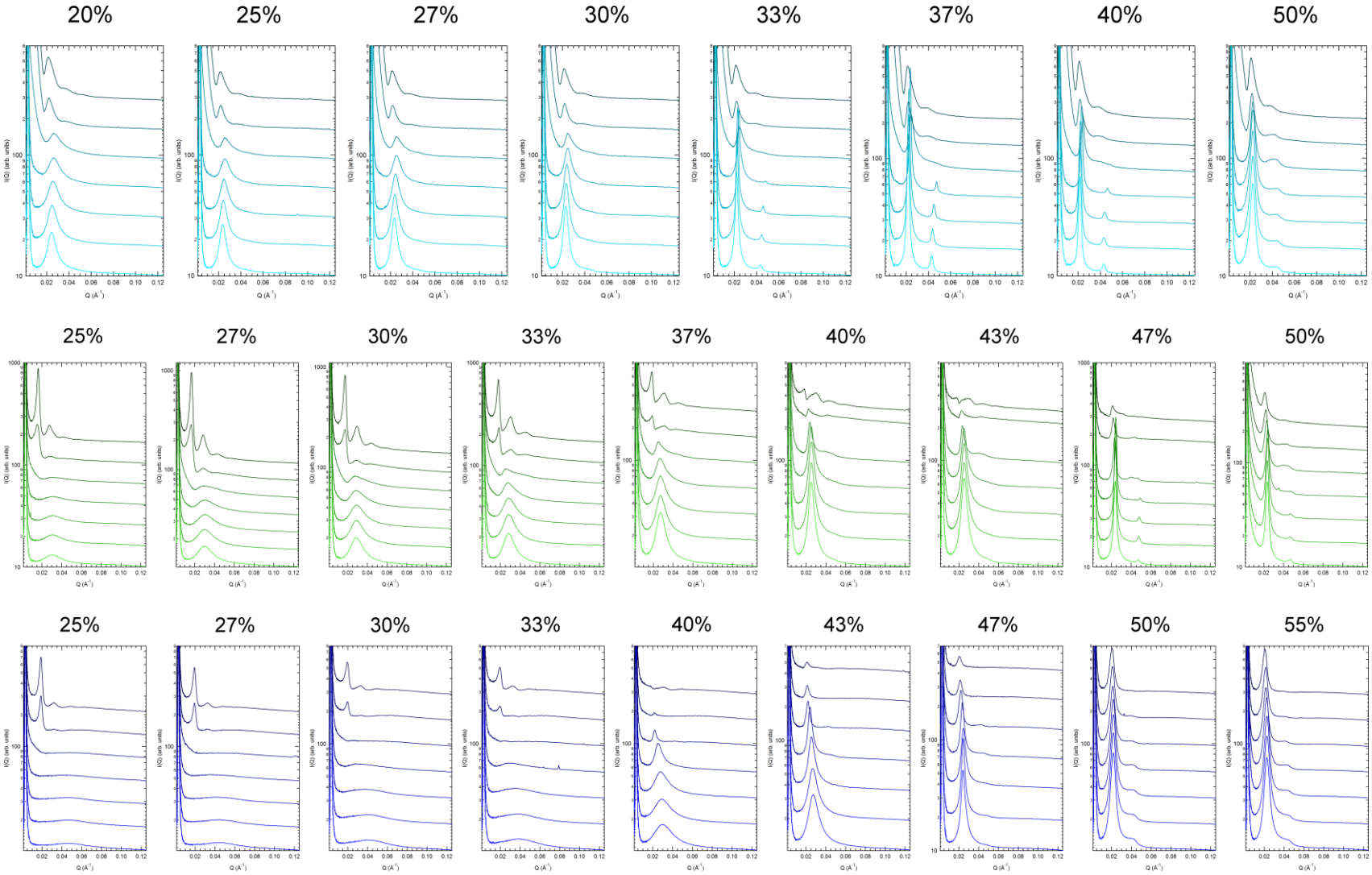

Figure S14. Radially averaged SAXS patterns for (top) GFP(0)-PNIPAM30k, (middle) GFP(-8)-PNIPAM30k, and (bottom) (GFP(-21)-PNIPAM30k. The curves are offset vertically for clarity. The seven curves in each plot increase in temperature upward from 10 to 40 °C in 5 °C intervals.

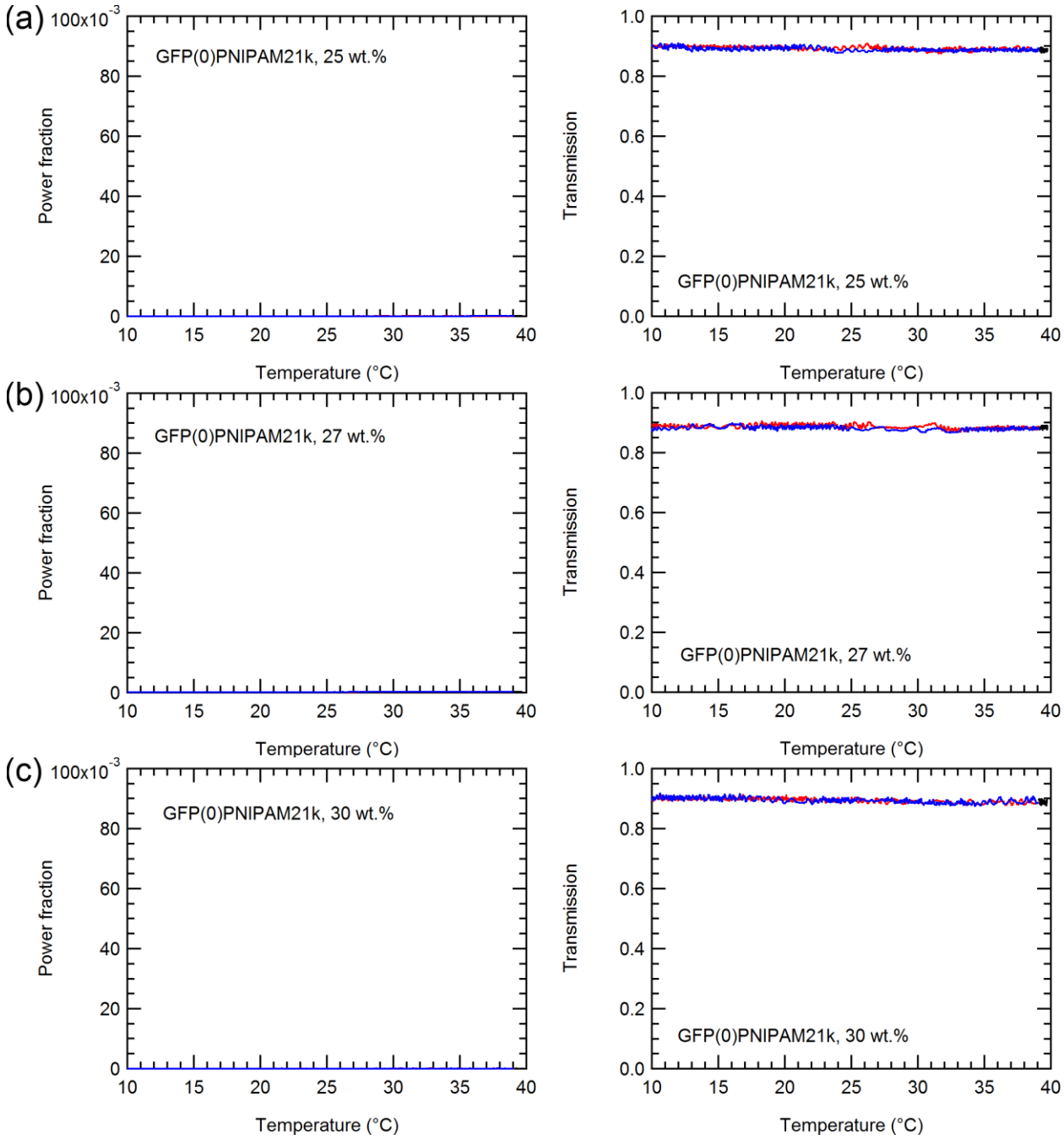

Figure S15 a-c. DPLS and turbidimetry of GFP(0)-PNIPAM21k at (a) 25 wt.%, (b) 27 wt.%, and (c) 30 wt.%. The red curve represents the heating cycle, and the blue curve represents the cooling cycle. The black curve represents the 10-minute equilibration at the end of the heating cycle before cooling.

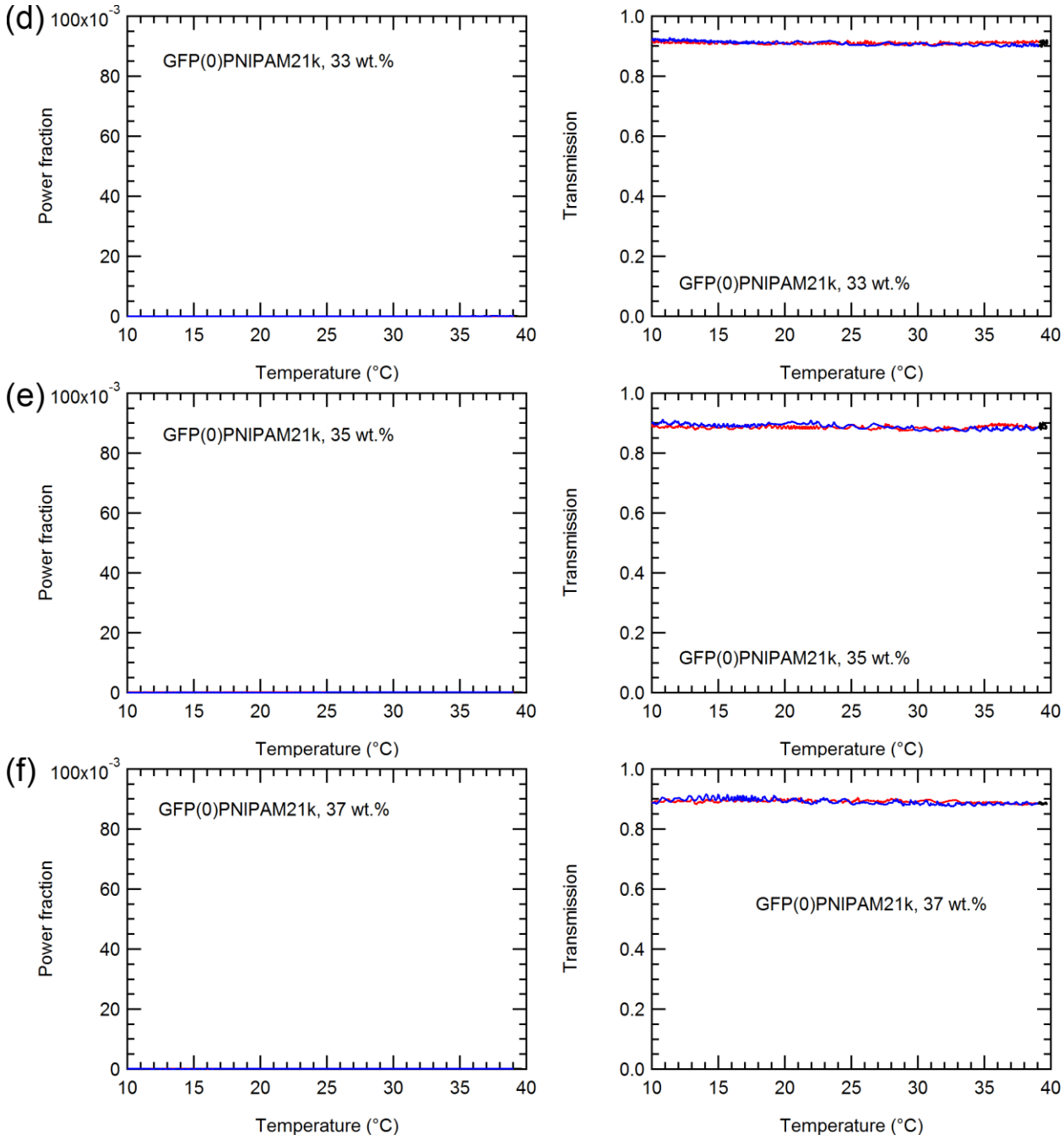

Figure S15 d-f. DPLS and turbidimetry of GFP(0)-PNIPAM21k at (d) 33 wt.%, (e) 35 wt.%, and (f) 37 wt.%. The red curve represents the heating cycle, and the blue curve represents the cooling cycle. The black curve represents the 10-minute equilibration at the end of the heating cycle before cooling.

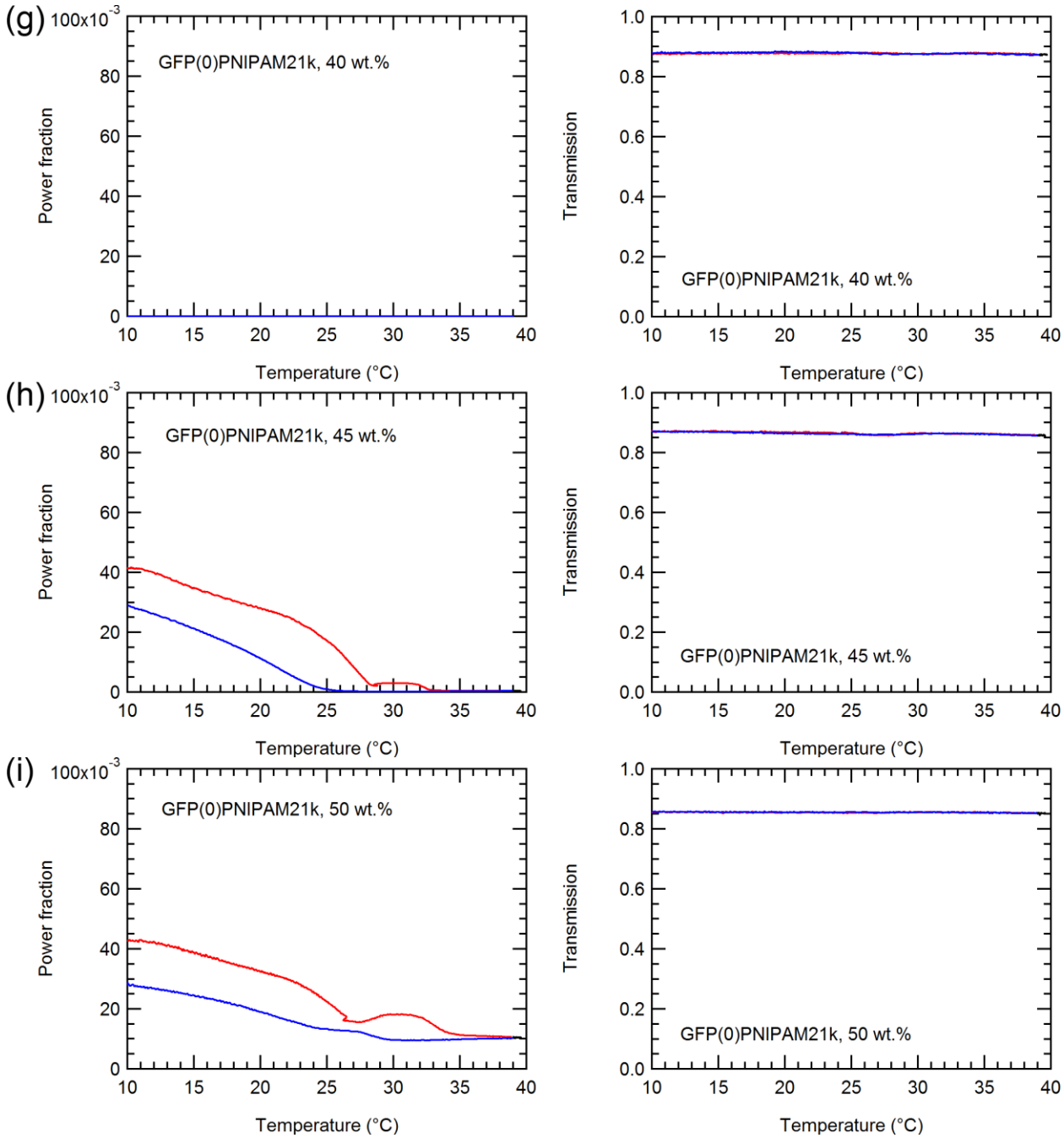

Figure S15 g-i. DPLS and turbidimetry of GFP(0)-PNIPAM21k at (g) 40 wt.%, (h) 45 wt.%, and (i) 50 wt.%. The red curve represents the heating cycle, and the blue curve represents the cooling cycle. The black curve represents the 10-minute equilibration at the end of the heating cycle before cooling.

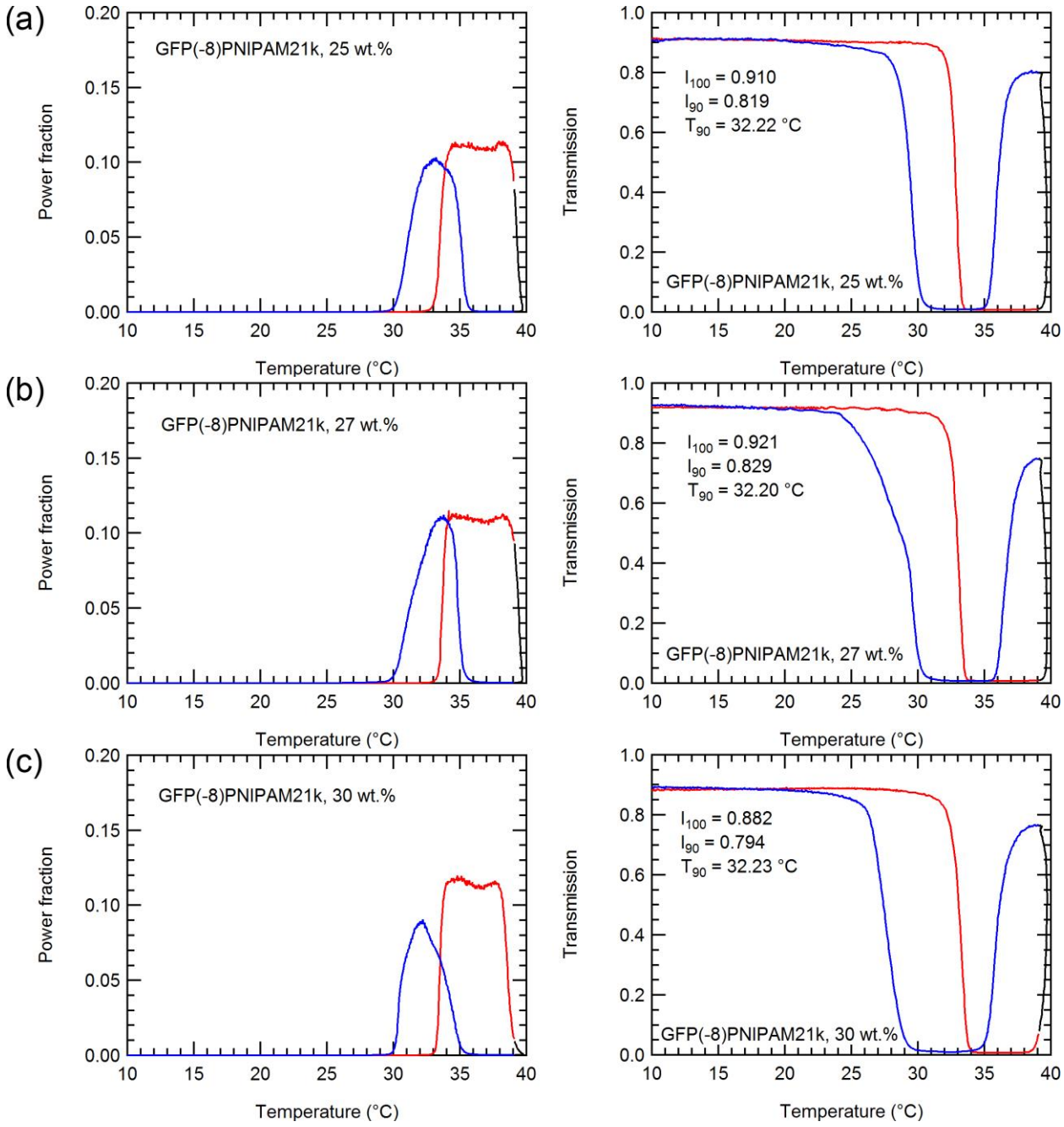

Figure S16 a-c. DPLS and turbidimetry of GFP(-8)-PNIPAM21k at (a) 25 wt.%, (b) 27 wt.%, and (c) 30 wt.%. The increase in power fraction at concentrations of 25-40 wt.% results from the decrease in transmission. The red curve represents the heating cycle, and the blue curve represents the cooling cycle. The black curve represents the 10-minute equilibration at the end of the heating cycle before cooling.

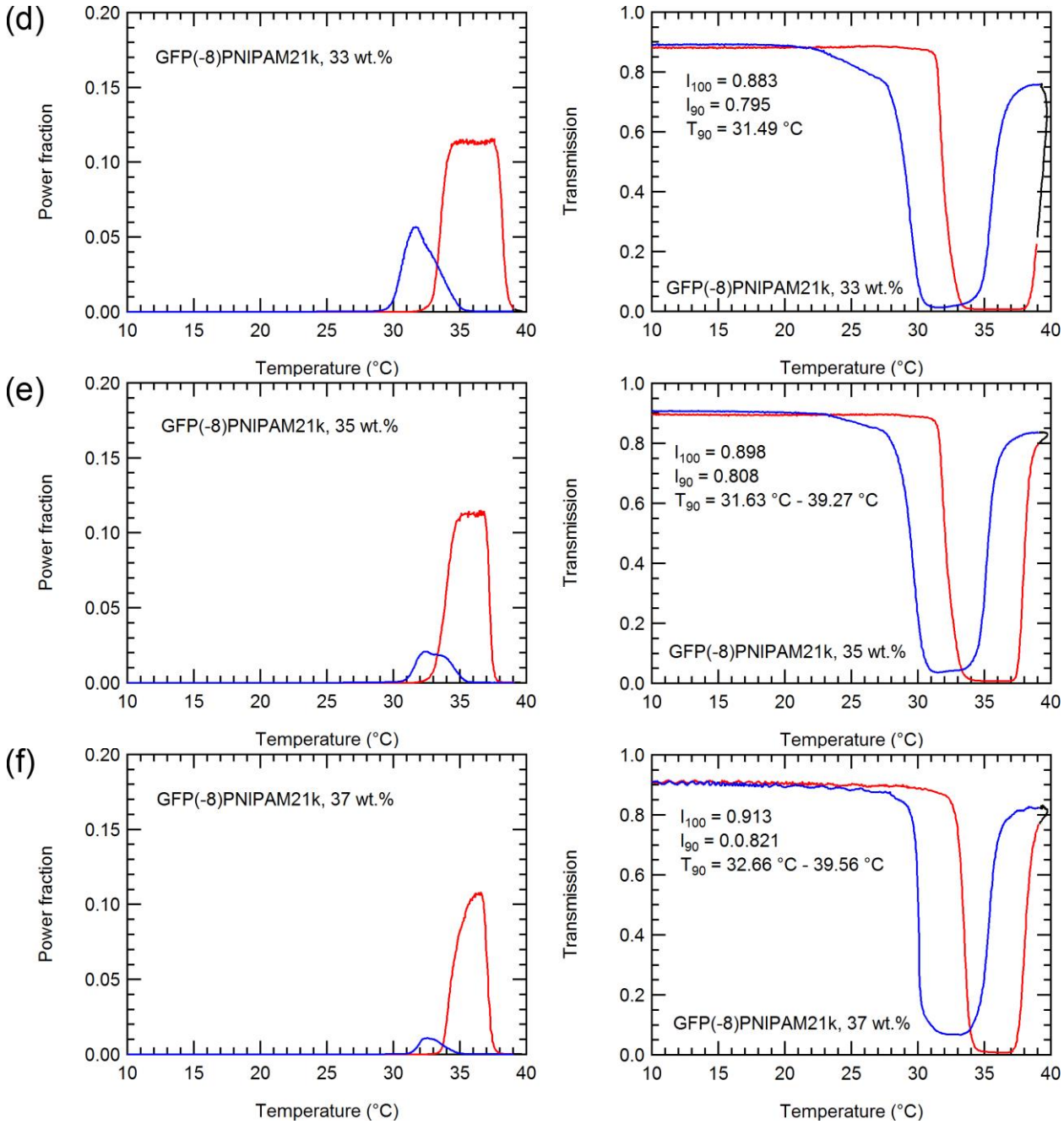

Figure S16 d-f. DPLS and turbidimetry of GFP(-8)-PNIPAM21k at (d) 33 wt.%, (e) 35 wt.%, and (f) 37 wt.%. The increase in power fraction at concentrations of 25-40 wt.% results from the decrease in transmission. The red curve represents the heating cycle, and the blue curve represents the cooling cycle. The black curve represents the 10-minute equilibration at the end of the heating cycle before cooling.

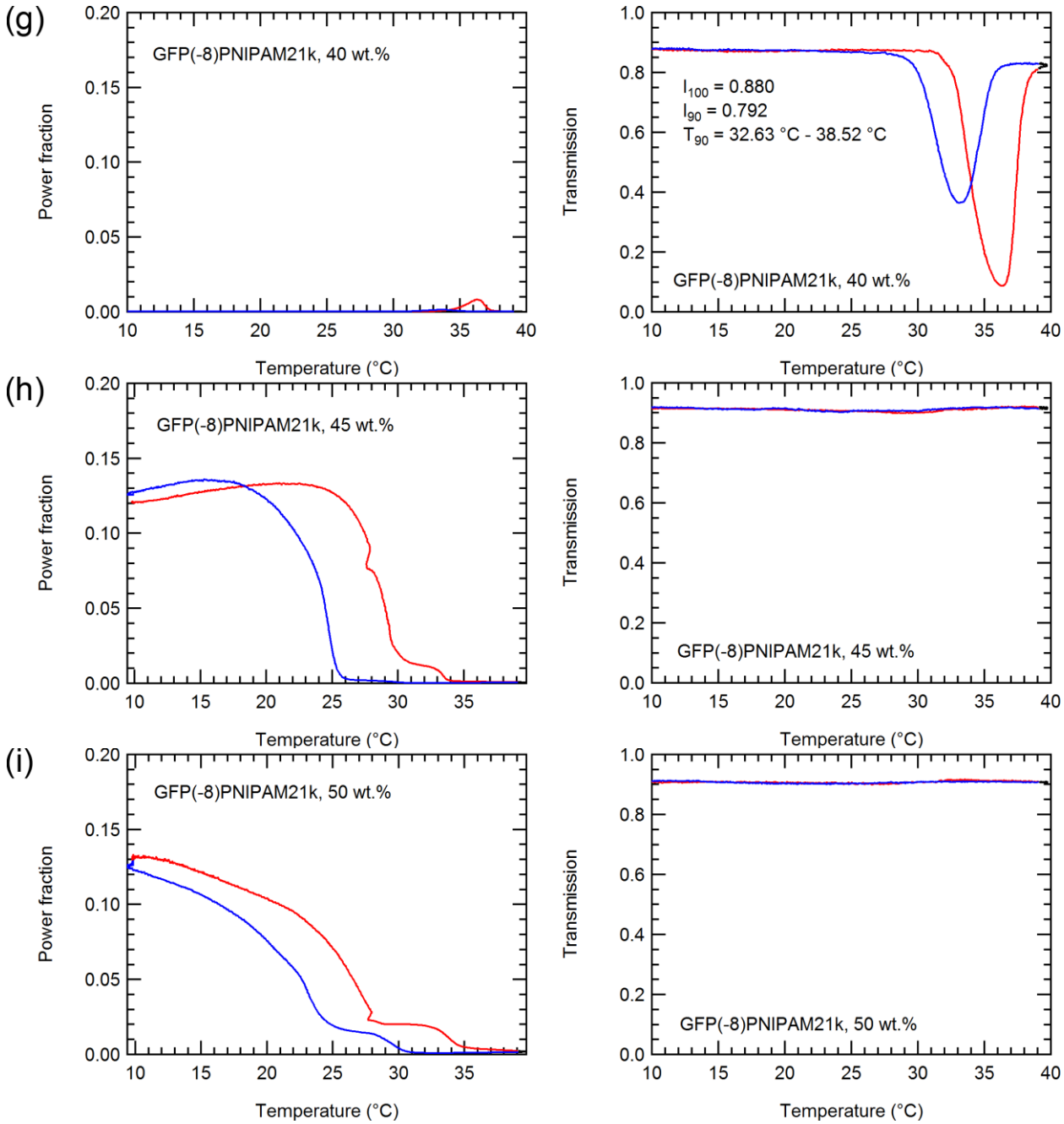

Figure S16 g-i. DPLS and turbidimetry of GFP(-8)-PNIPAM21k at (g) 40 wt.%, (h) 45 wt.%, and (i) 50 wt.%. The increase in power fraction at concentrations of 25-40 wt.% results from the decrease in transmission. The red curve represents the heating cycle, and the blue curve represents the cooling cycle. The black curve represents the 10-minute equilibration at the end of the heating cycle before cooling.

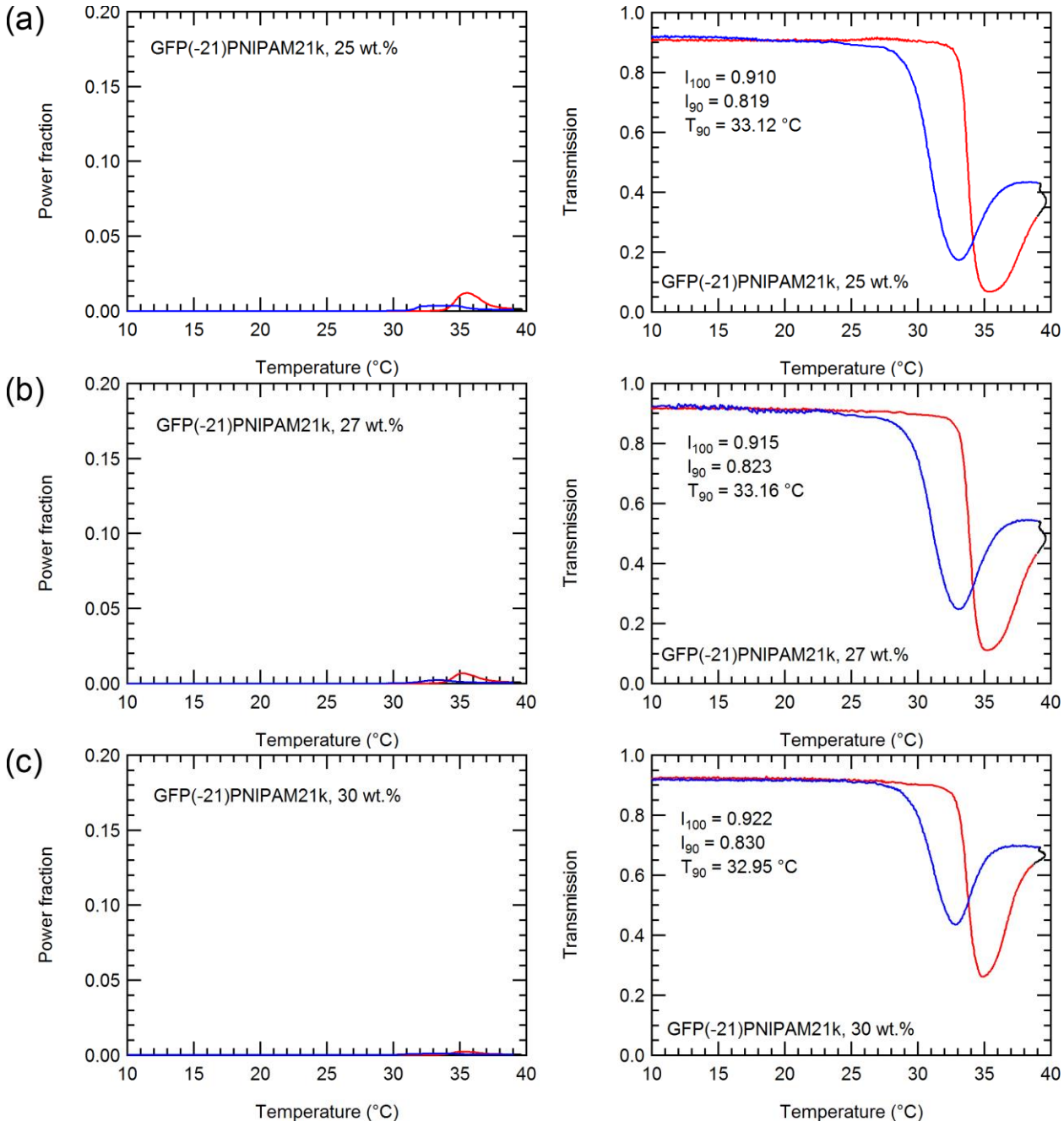

Figure S17 a-c. DPLS and turbidimetry of GFP(-21)-PNIPAM21k at (a) 25 wt.%, (b) 27 wt.%, and (c) 30 wt.%. The red curve represents the heating cycle, and the blue curve represents the cooling cycle. The black curve represents the 10-minute equilibration at the end of the heating cycle before cooling.

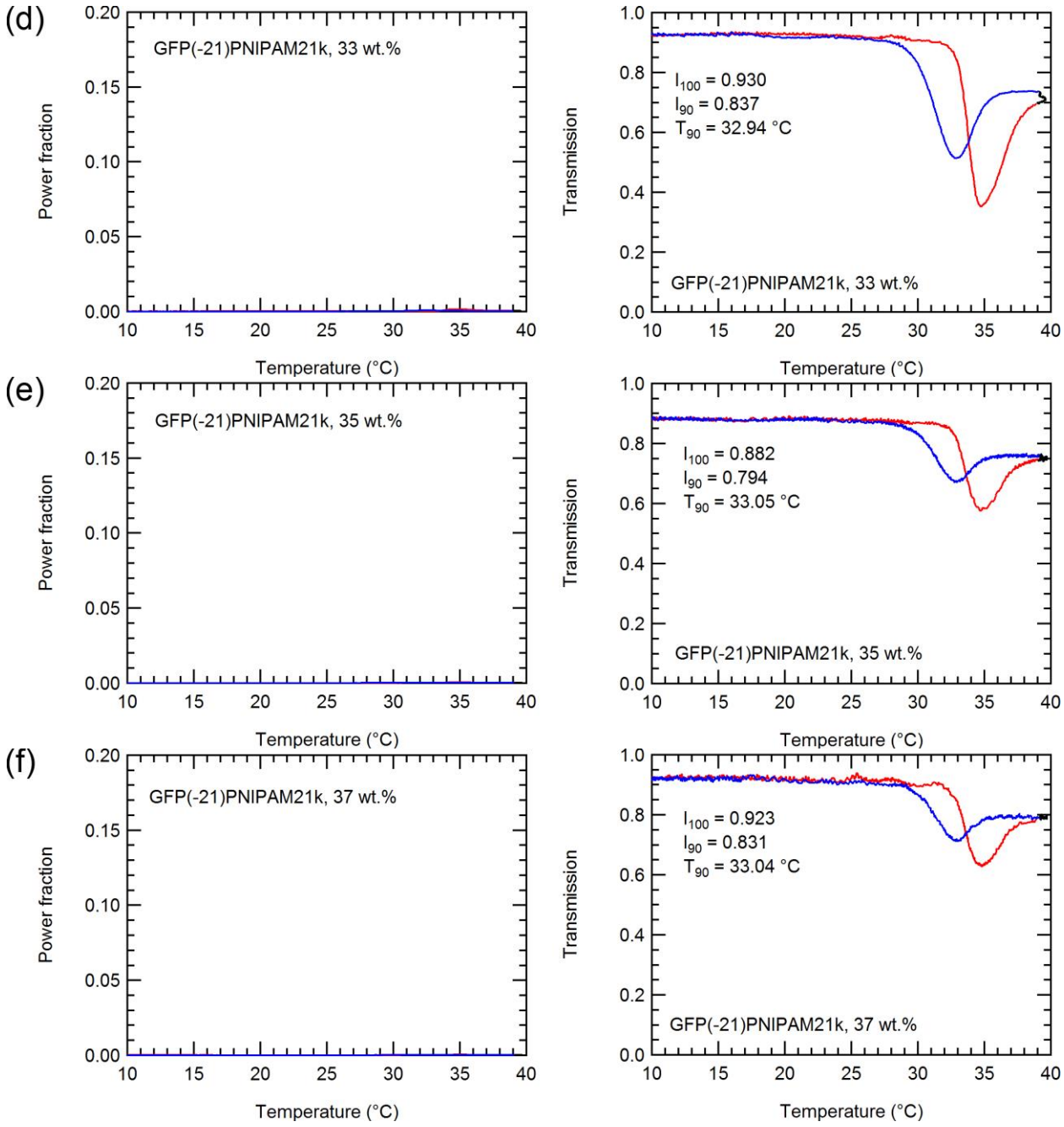

Figure S17 d-f. DPLS and turbidimetry of GFP(-21)-PNIPAM21k at (d) 33 wt.%, (e) 35 wt.%, and (f) 37 wt.%. The red curve represents the heating cycle, and the blue curve represents the cooling cycle. The black curve represents the 10-minute equilibration at the end of the heating cycle before cooling.

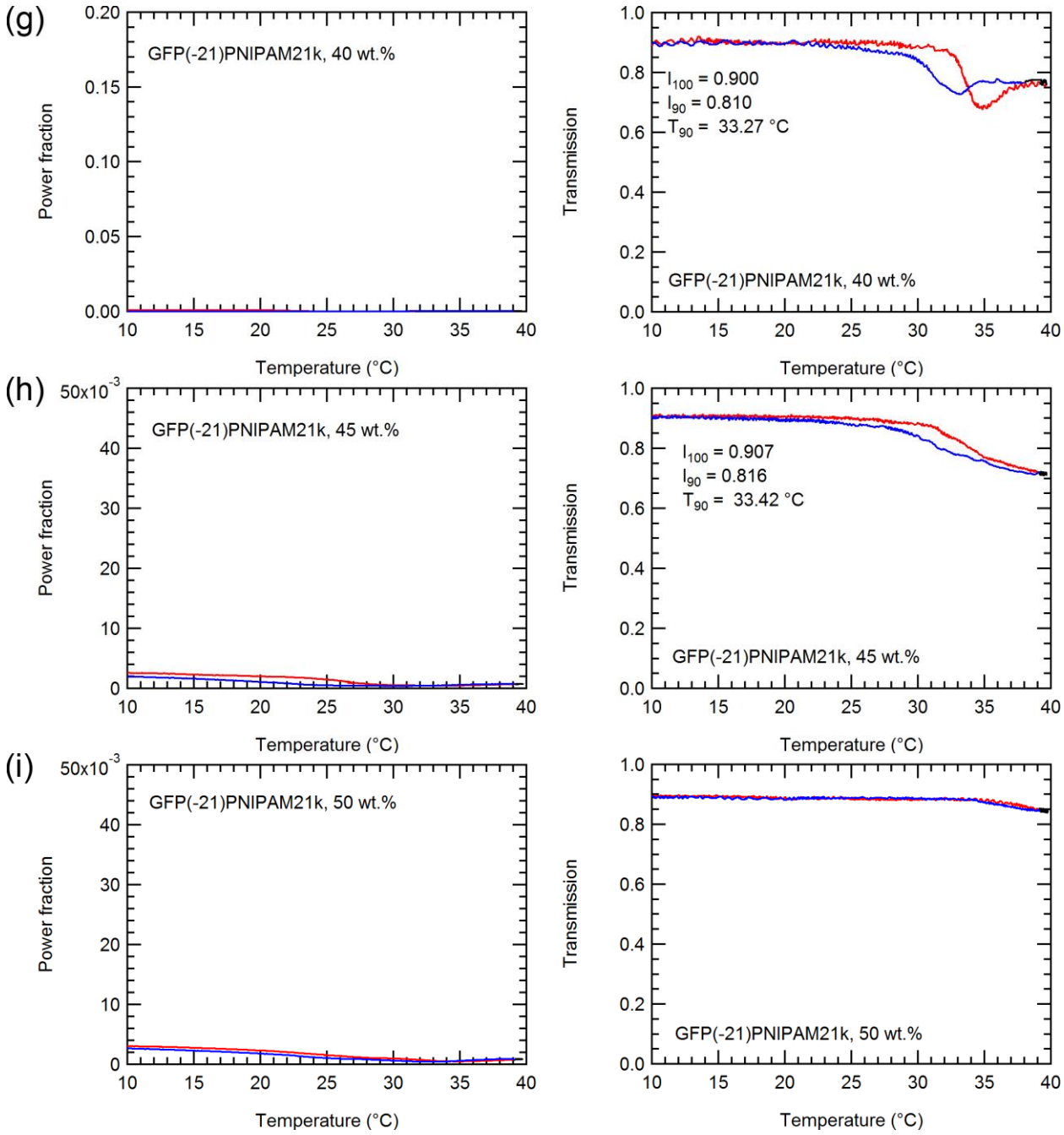

Figure S17 g-i. DPLS and turbidimetry of GFP(-21)-PNIPAM21k at (g) 40 wt.%, (h) 45 wt.%, and (i) 50 wt.%. The red curve represents the heating cycle, and the blue curve represents the cooling cycle. The black curve represents the 10-minute equilibration at the end of the heating cycle before cooling.

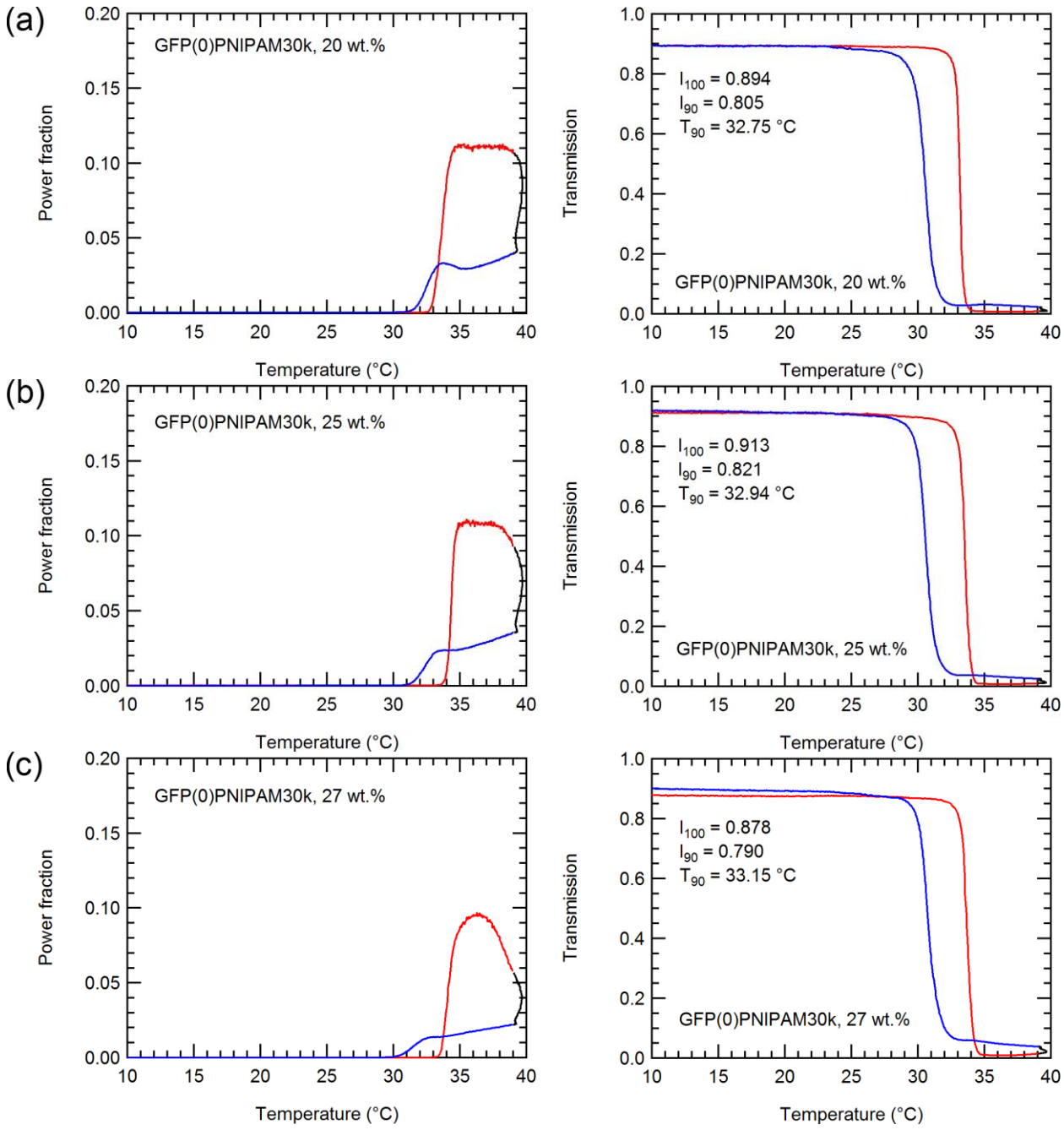

Figure S18 a-c. DPLS and turbidimetry of GFP(0)-PNIPAM30k at (a) 20 wt.%, (b) 25 wt.%, and (c) 27 wt.%. The sharp drop in transmission results in the increase in power fraction at high temperature. The birefringence results can only be interpreted up to the thermal transition temperature. The red curve represents the heating cycle, and the blue curve represents the cooling cycle. The black curve represents the 10-minute equilibration at the end of the heating cycle before cooling.

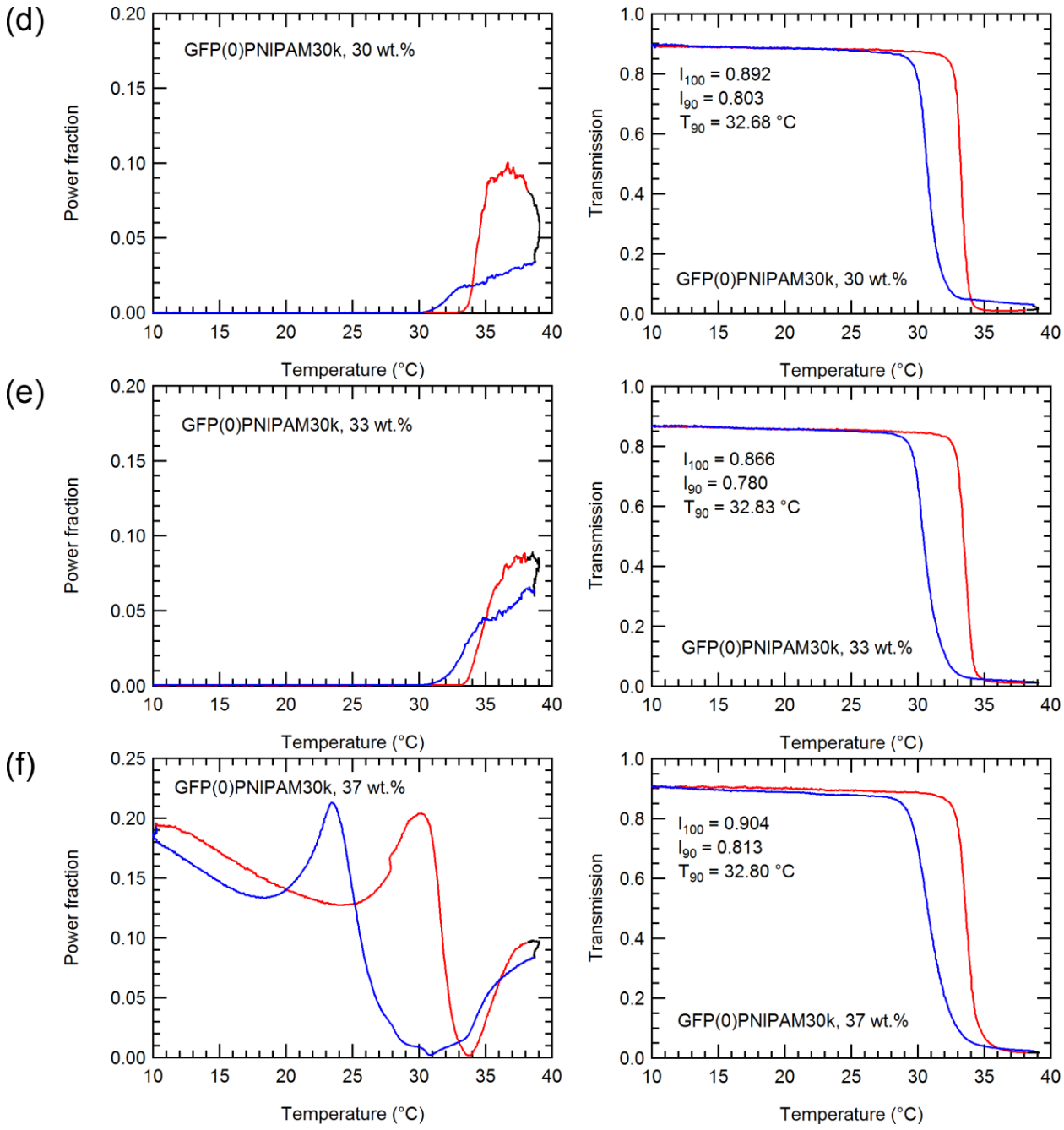

Figure S18 d-f. DPLS and turbidimetry of GFP(0)-PNIPAM30k at (d) 30 wt.%, (e) 33 wt.%, and (f) 37 wt.%. The sharp drop in transmission results in the increase in power fraction at high temperature. The birefringence results can only be interpreted up to the thermal transition temperature. The red curve represents the heating cycle, and the blue curve represents the cooling cycle. The black curve represents the 10-minute equilibration at the end of the heating cycle before cooling.

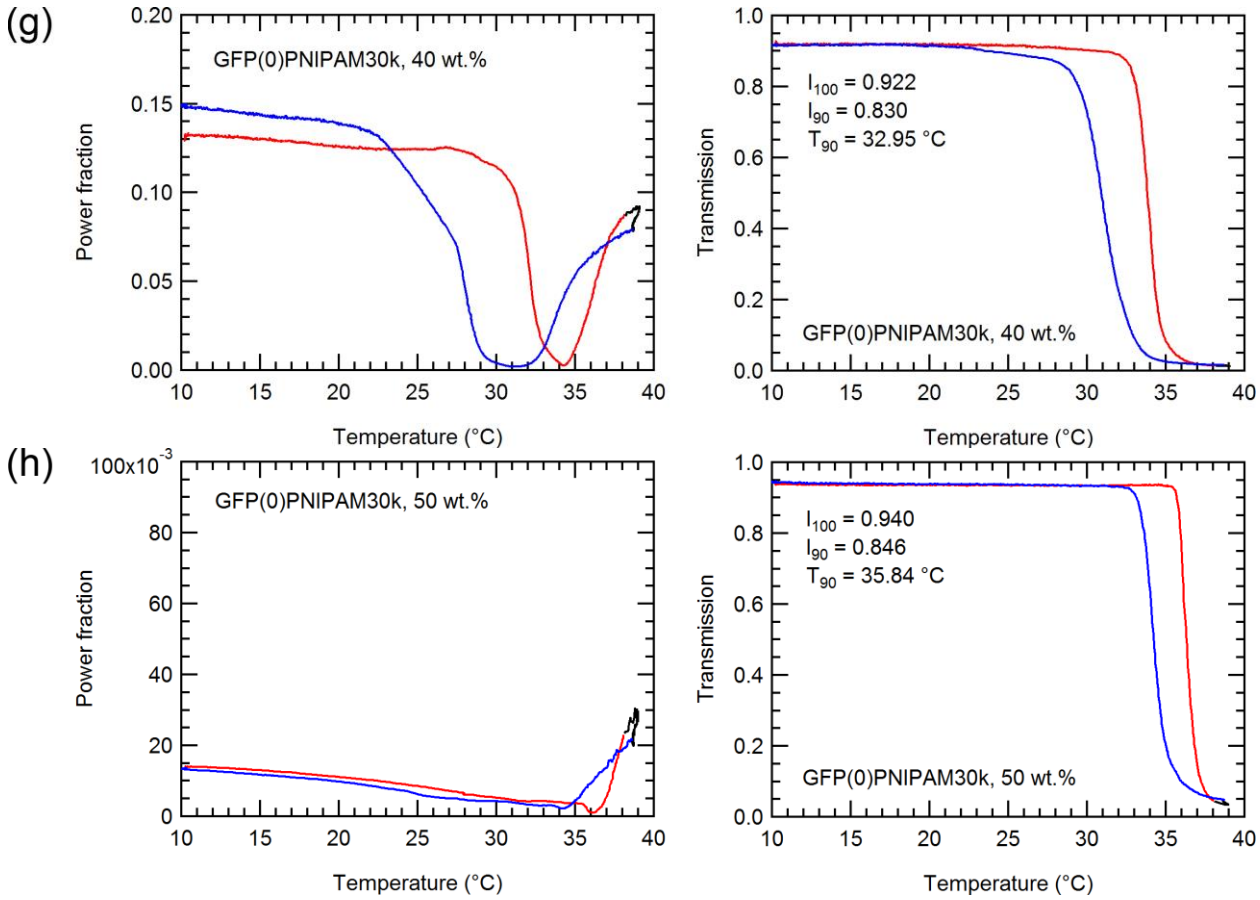

Figure S18 g-h. DPLS and turbidimetry of GFP(0)-PNIPAM30k at (g) 40 wt.% and (h) 50 wt.%. The sharp drop in transmission results in the increase in power fraction at high temperature. The birefringence results can only be interpreted up to the thermal transition temperature. The red curve represents the heating cycle, and the blue curve represents the cooling cycle. The black curve represents the 10-minute equilibration at the end of the heating cycle before cooling.

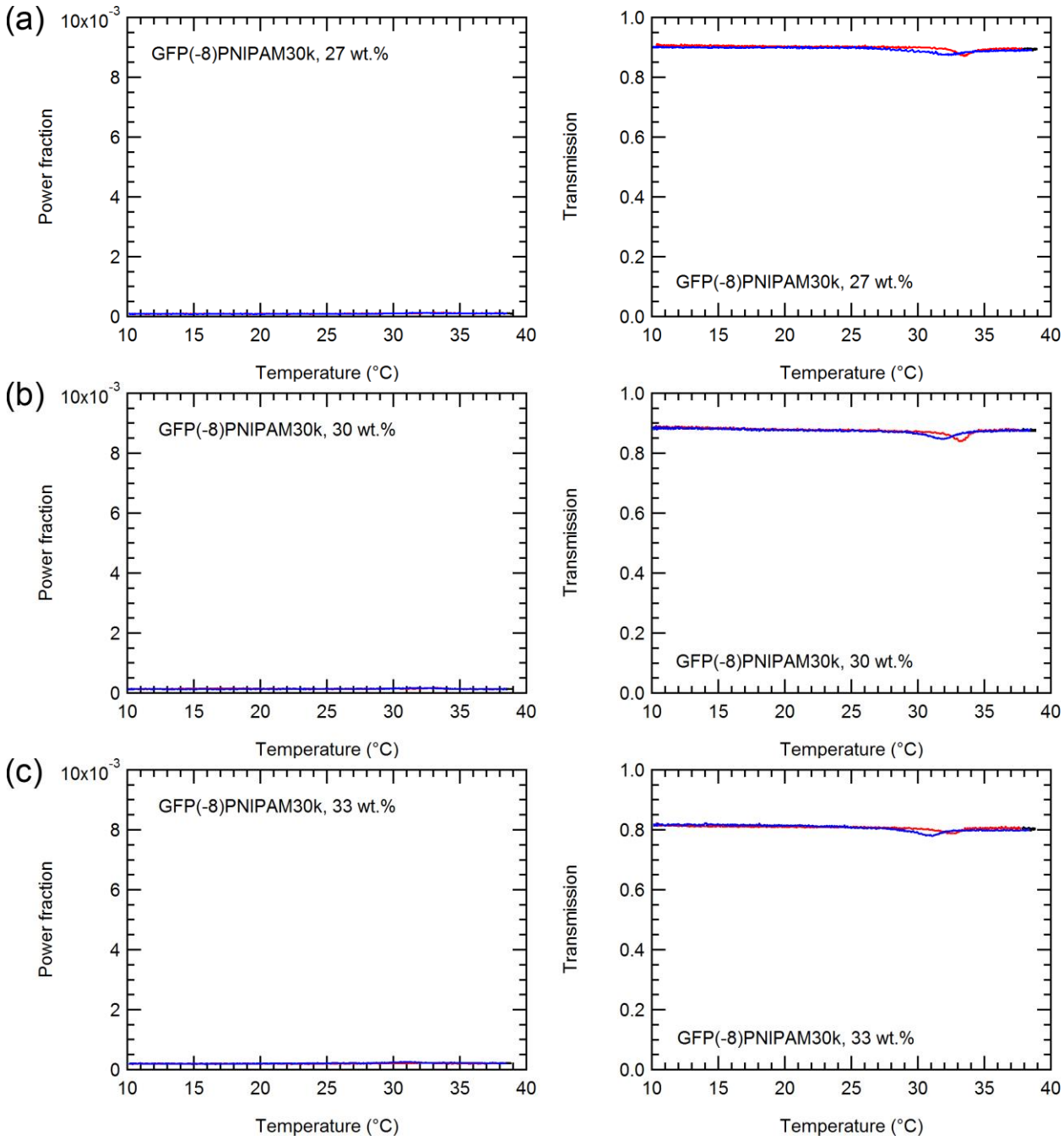

Figure S19 a-c. DPLS and turbidimetry of GFP(-8)-PNIPAM30k at (a) 27 wt.%, (b) 30 wt.%, and (c) 33 wt.%. The red curve represents the heating cycle, and the blue curve represents the cooling cycle. The black curve represents the 10-minute equilibration at the end of the heating cycle before cooling.

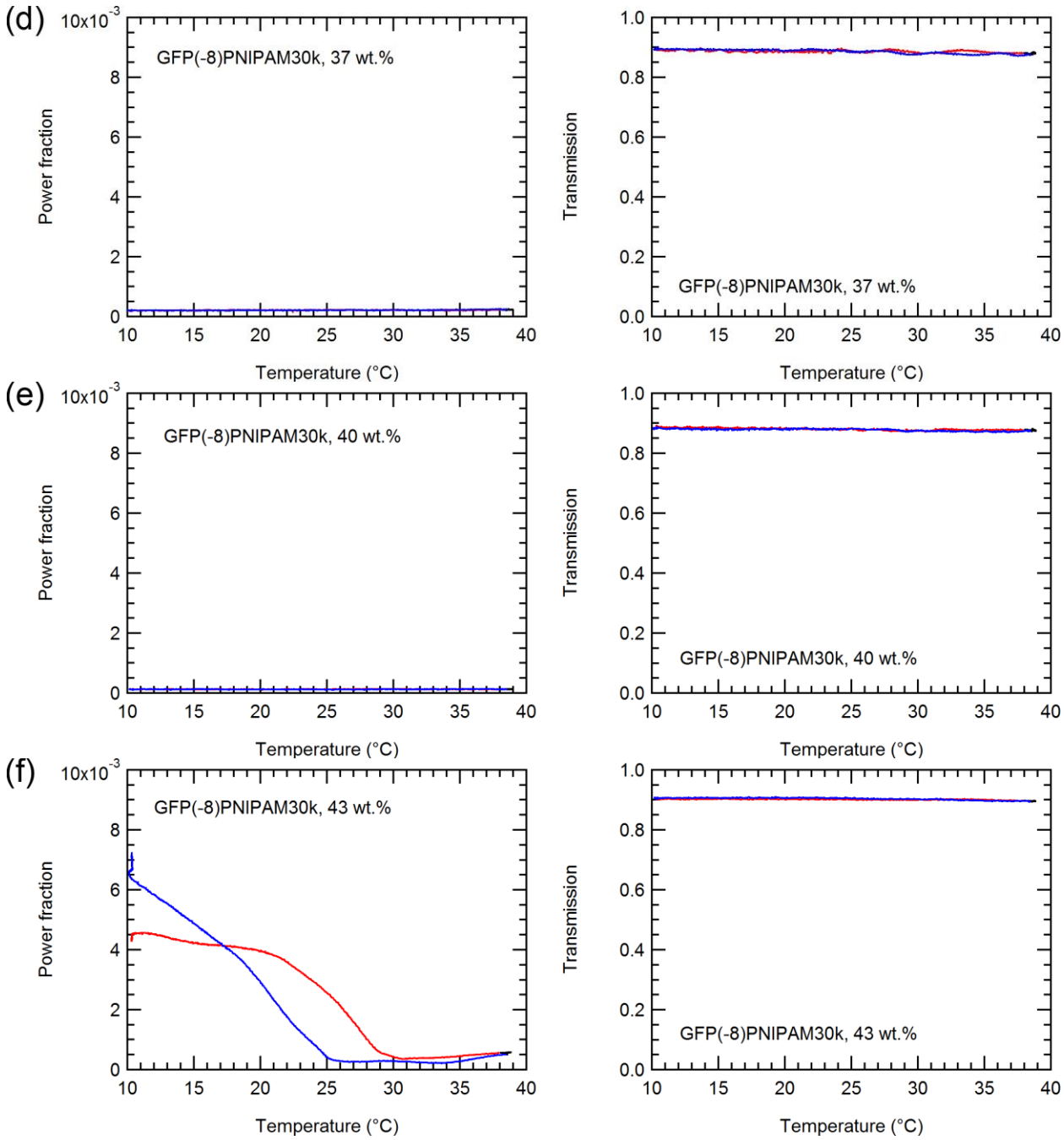

Figure S19 d-f. DPLS and turbidimetry of GFP(-8)-PNIPAM30k at (d) 37 wt.%, (e) 40 wt.%, and (f) 43 wt.%. The red curve represents the heating cycle, and the blue curve represents the cooling cycle. The black curve represents the 10-minute equilibration at the end of the heating cycle before cooling.

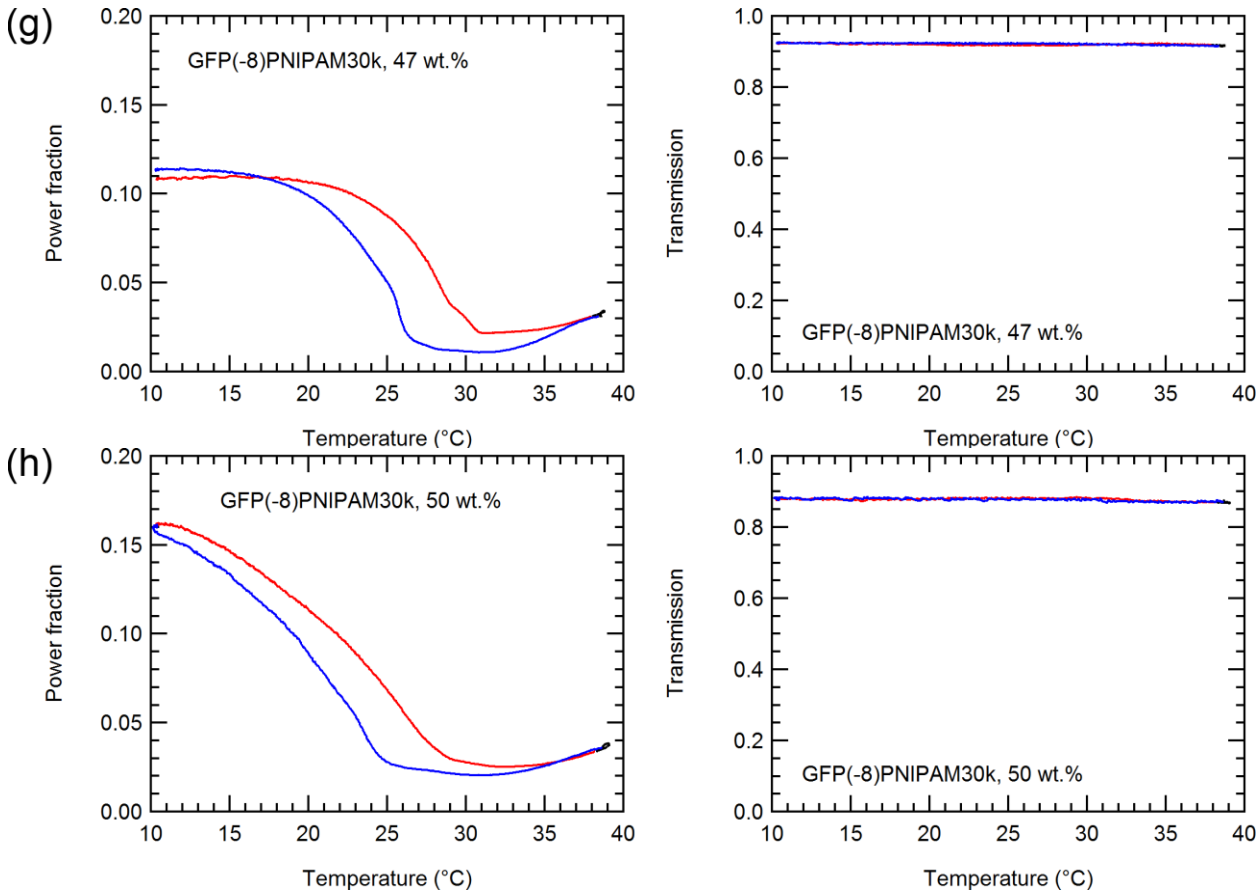

Figure S19 g-h. DPLS and turbidimetry of GFP(-8)-PNIPAM30k at (g) 47 wt.% and (h) 50 wt.%. The red curve represents the heating cycle, and the blue curve represents the cooling cycle. The black curve represents the 10-minute equilibration at the end of the heating cycle before cooling.

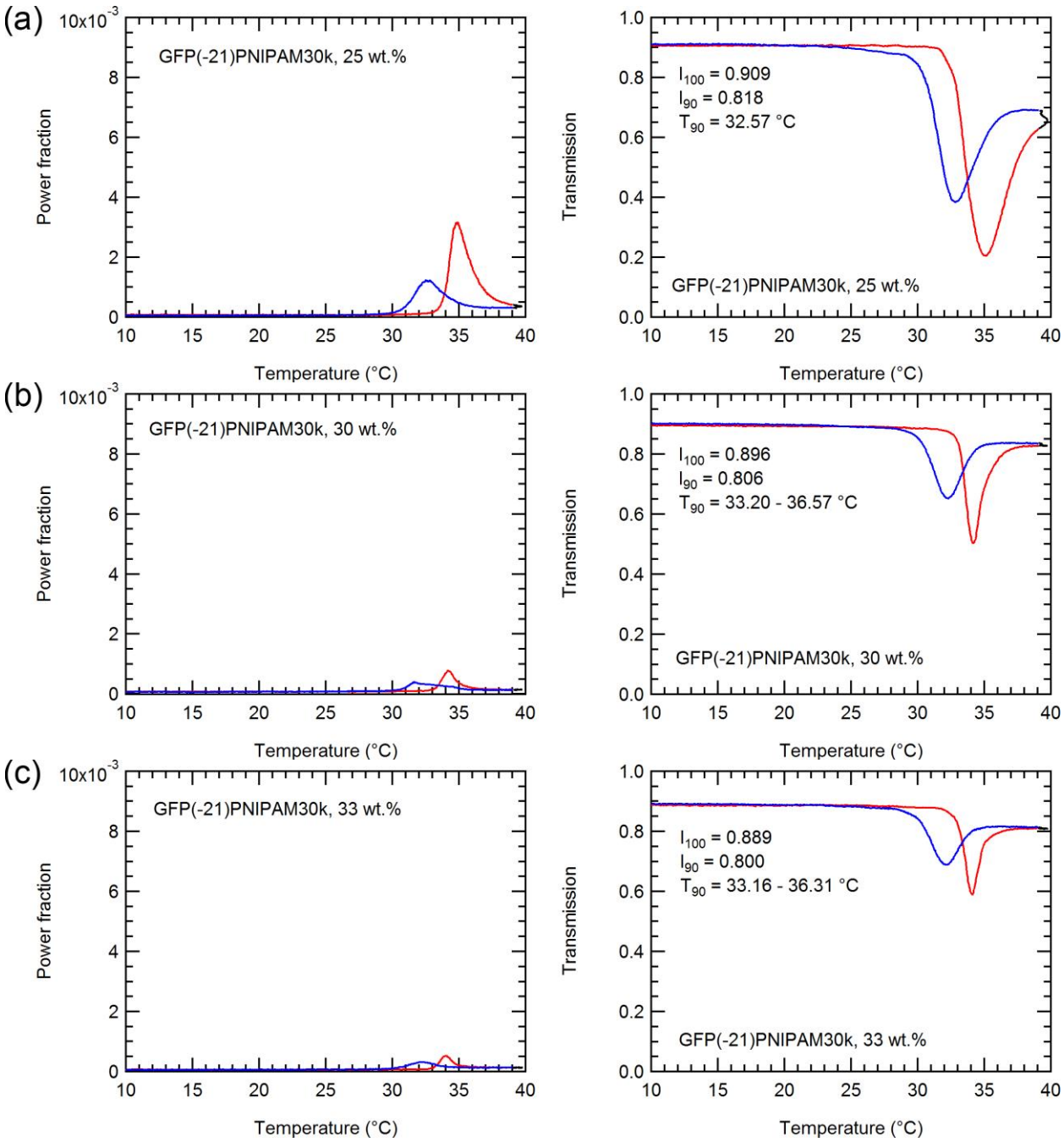

Figure S20 a-c. DPLS and turbidimetry of GFP(-21)-PNIPAM30k at (a) 25 wt.%, (b) 30 wt.%, and (c) 33 wt.%. The moderate increases in power fraction result from the moderate decrease in transmission. The red curve represents the heating cycle, and the blue curve represents the cooling cycle. The black curve represents the 10-minute equilibration at the end of the heating cycle before cooling.

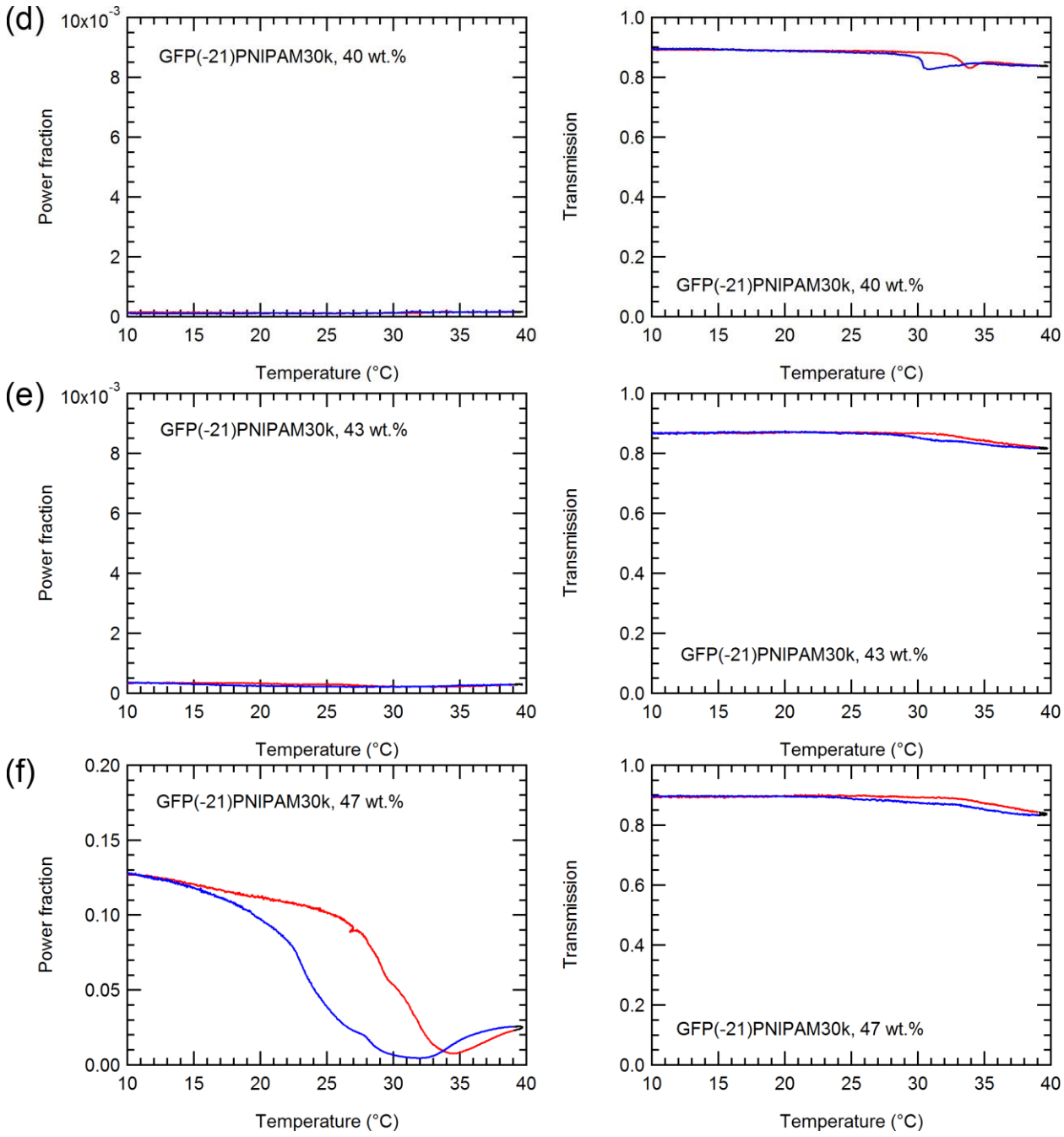

Figure S20 d-f. DPLS and turbidimetry of GFP(-21)-PNIPAM30k at (d) 40 wt.%, (e) 43 wt.%, and (f) 47 wt.%. The red curve represents the heating cycle, and the blue curve represents the cooling cycle. The black curve represents the 10-minute equilibration at the end of the heating cycle before cooling.

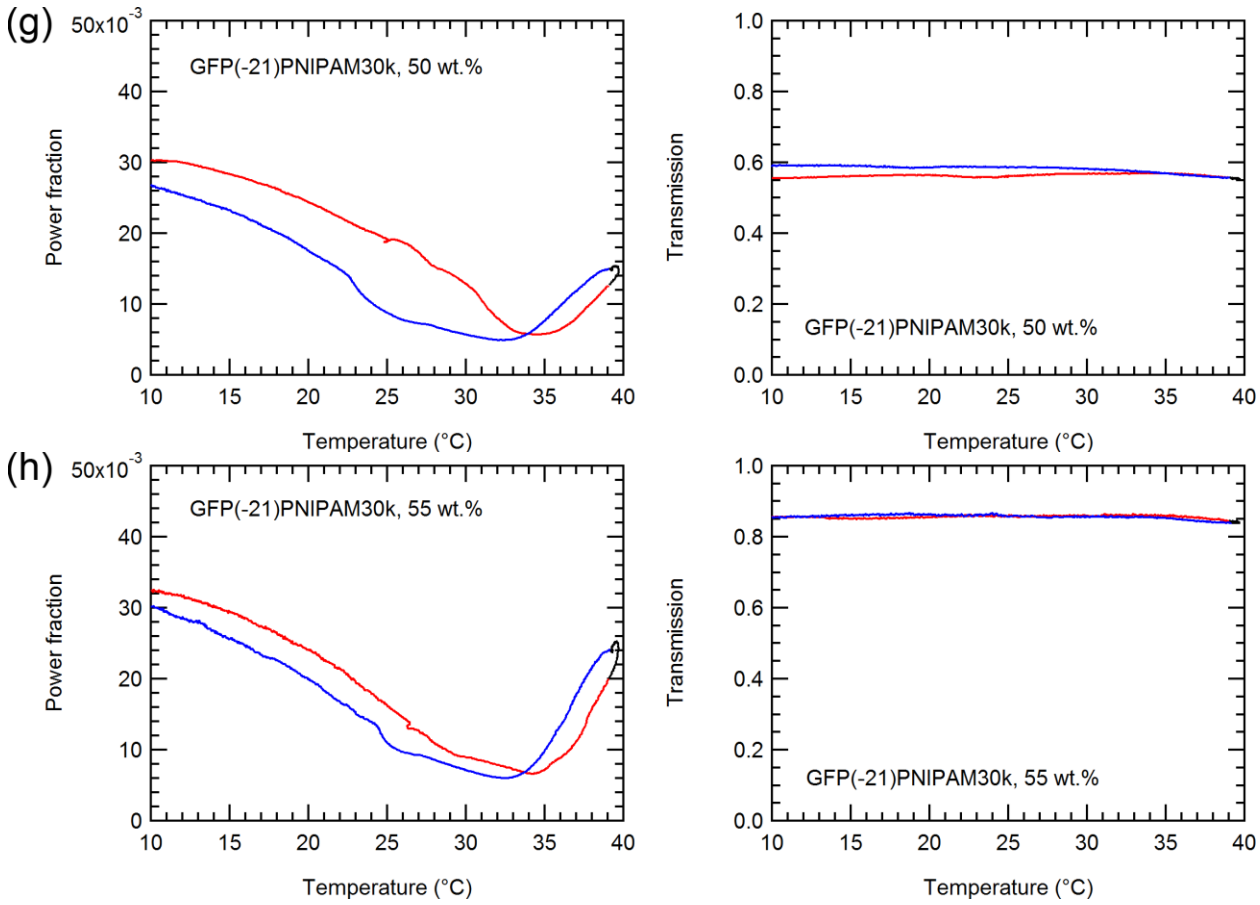

Figure S20 g-h. DPLS and turbidimetry of GFP(-21)-PNIPAM30k at (g) 50 wt.% and (h) 55 wt.%. The red curve represents the heating cycle, and the blue curve represents the cooling cycle. The black curve represents the 10-minute equilibration at the end of the heating cycle before cooling.

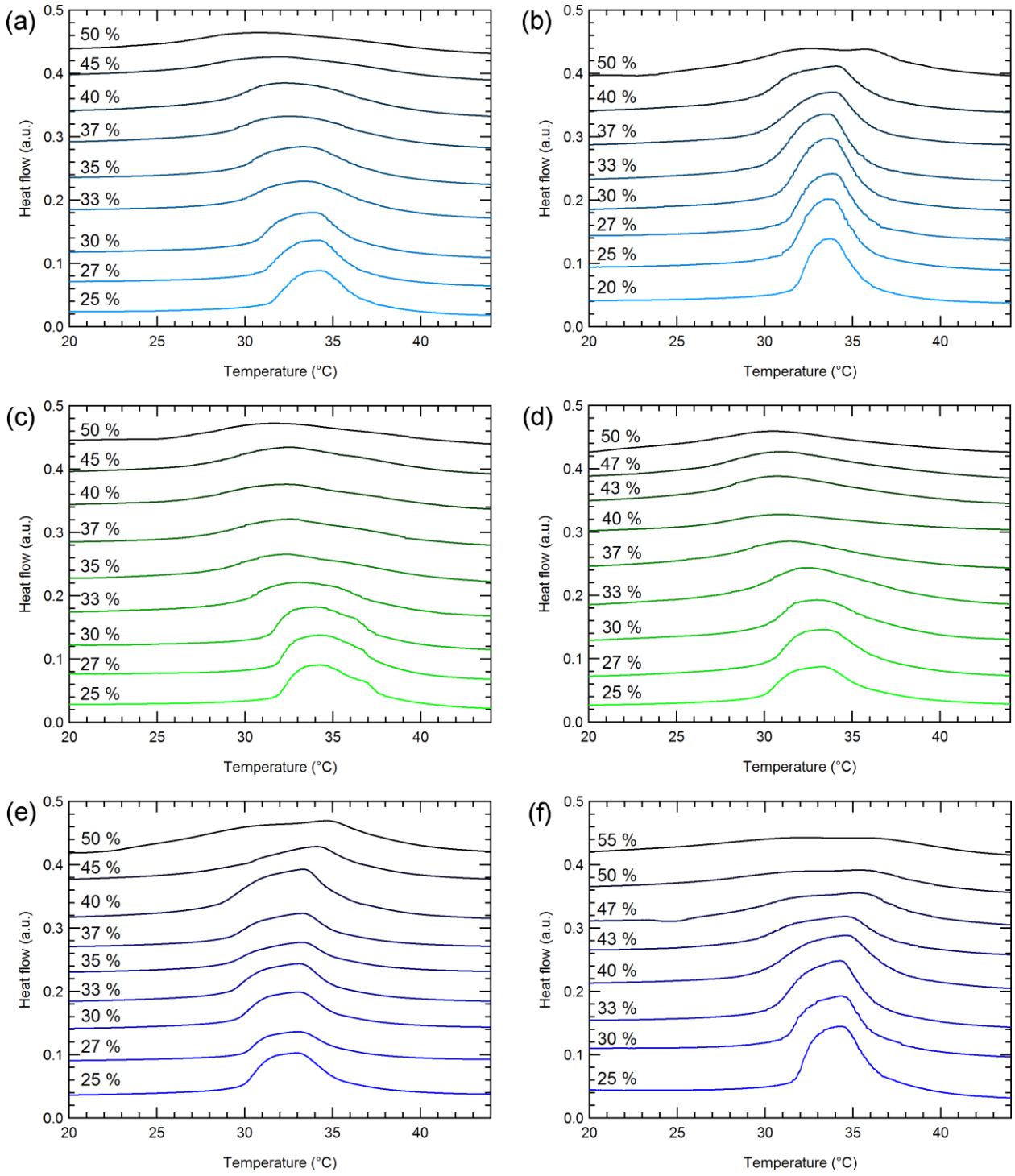

Figure S21. DSC of (a) GFP(0)-PNIPAM21k, (b) GFP(0)-PNIPAM30k, (c) GFP(-8)-PNIPAM21k, (d) GFP(-8)-PNIPAM30k, (e) GFP(-21)-PNIPAM21k, and (f) GFP(-21)-PNIPAM30k.

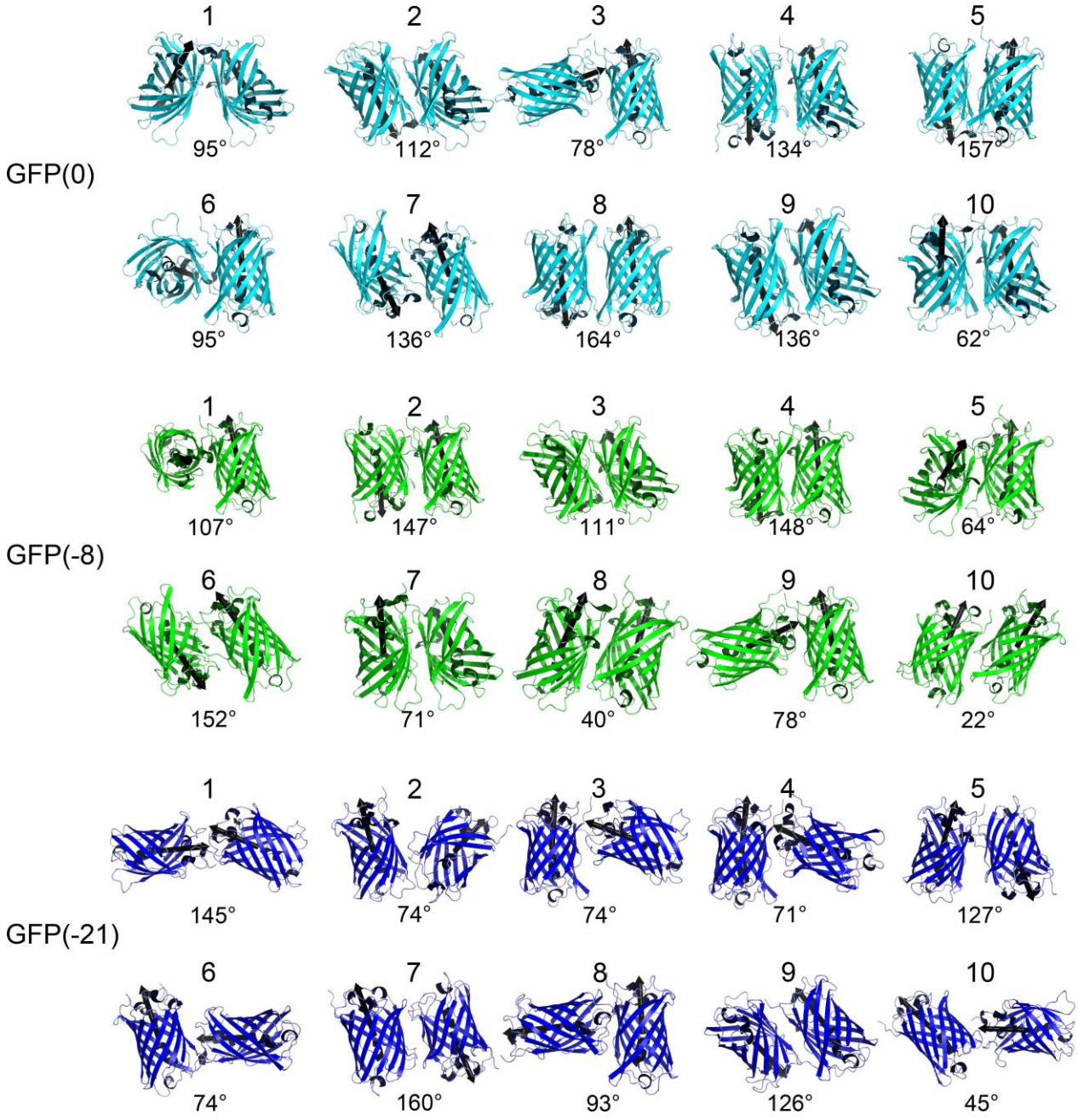

Figure S22. Cartoon schematic representations of results from ClusPro 2.0[8,9] of the ten largest clusters representing the most probable configurations for interactions between two GFP molecules as a function of total net charge. The orientation angle between proteins is displayed underneath each configuration and is calculated as the angle between the vectors in the directions of the principal axes aligned with the beta barrel of the two proteins, represented as the black arrows. The cluster size and corresponding energy for these clusters are displayed in Table S1.

Table S1. Tabulated values for cluster scores from ClusPro 2.0 of the ten largest clusters representing the most probable configurations for interactions between two GFP molecules as a function of total net charge.

	GFP(0)			**GFP(-8)**			**GFP(-21)**		
Cluster	Members	Representative	Weighted Score	Members	Representative	Weighted Score	Members	Representative	Weighted Score
1	134	Center	-505.1	136	Center	-588.5	52	Center	-433.3
		Lowest energy	-614.1		Lowest energy	-615.0		Lowest energy	-433.3
2	53	Center	-612.1	70	Center	-566.4	48	Center	-387.2
		Lowest energy	-628.5		Lowest energy	-566.4		Lowest energy	-447.0
3	50	Center	-569.3	58	Center	-616.5	47	Center	-447.3
		Lowest energy	-569.3		Lowest energy	-616.5		Lowest energy	-447.3
4	47	Center	-541.2	44	Center	-501.7	43	Center	-446.5
		Lowest energy	-541.2		Lowest energy	-544.3		Lowest energy	-446.5
5	43	Center	-473.9	37	Center	-495.6	39	Center	-398.1
		Lowest energy	-546.6		Lowest energy	-557.7		Lowest energy	-449.5
6	41	Center	-532.2	36	Center	-510.7	35	Center	-437.9
		Lowest energy	-613.4		Lowest energy	-532.1		Lowest energy	-437.9
7	33	Center	-504.5	36	Center	-510.8	33	Center	-404.7
		Lowest energy	-524.6		Lowest energy	-587.0		Lowest energy	-437.3
8	33	Center	-571.2	36	Center	-531.8	33	Center	-489.2
		Lowest energy	-571.2		Lowest energy	-601.3		Lowest energy	-489.2
9	29	Center	-475.8	34	Center	-536.1	32	Center	-436.9
		Lowest energy	-606.6		Lowest energy	-536.1		Lowest energy	-469.3
10	29	Center	-539.2	30	Center	-538.1	32	Center	-393.9
		Lowest energy	-562.2		Lowest energy	-538.1		Lowest energy	-429.3

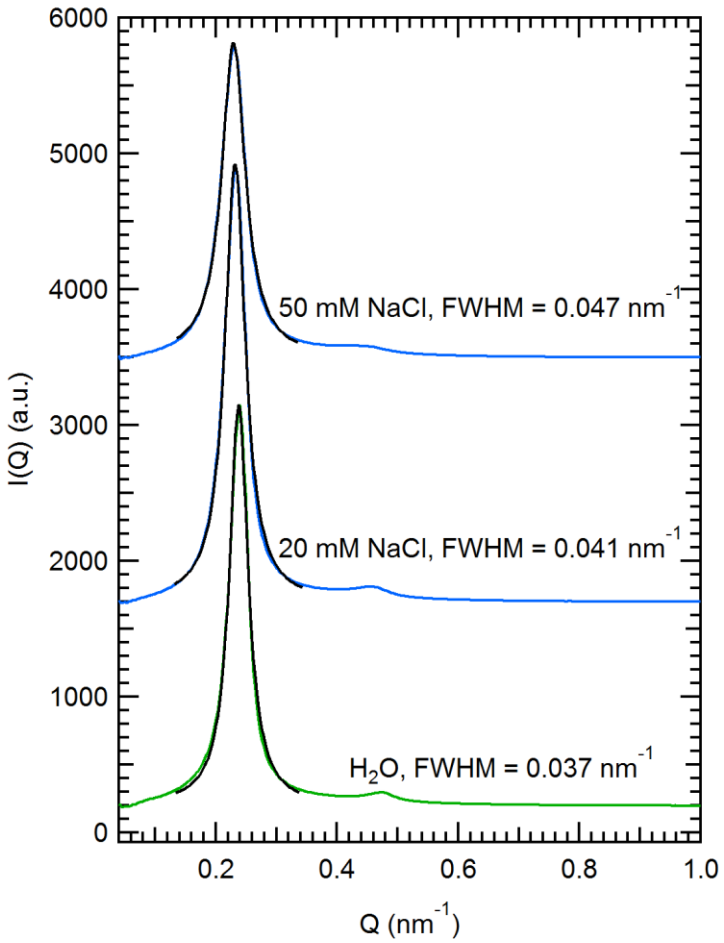

Figure S23. SAXS patterns of GFP(-21), ϕ_{PNIPAM} = 0.60, at 47 wt.% show lamellar morphologies in water and in the presence of NaCl at 20 and 50 mM. FWHM values of the primary peak from fitting a Lorentzian show that NaCl is not observed to improve the ordering relative to the self-assembly in H_2O.

Estimation of maximum counterion concentration for GFP(-21)-PNIPAM

The effect of divalent cations on the self-assembly of GFP(-21)-PNIPAM, ϕ_{PNIPAM} = 0.60, is studied at the C_{ODT} of 47 wt.%. Assuming a basis of 100 g, 47 g of GFP(-21)-PNIPAM, ϕ_{PNIPAM} = 0.60 corresponds to $\left(\frac{28,430}{28,430+30,720}\right)(47) = 22.6\,\text{g}$ of protein, with GFP(-21) having a molar mass of 28,430 g/mol and PNIPAM30k having a number average molar mass of 30,720 g/mol. Assuming an ideal solution and that the density of the conjugate is approximately 1 g cm^{-3}, this corresponds to 7.94 x 10^{-4} mol of protein and a concentration of $\left(\frac{7.94 \text{ x } 10^{-4}\text{ mol}}{0.100\text{ L}}\right) = 0.00794\text{ M}$ of GFP(-21). GFP(-21) has 22 positive residues and 43 negative residues. Assuming that charge neutrality is maintained with 22 molecules of NaCl for 22 positive and negative residues and an additional 21 Na^+ ions for the remaining 21 negative residues, the estimated total concentration of counterions is 0.516 M.

References

(1) Balsara, N. P.; Perahia, D.; Safinya, C. R.; Tirrell, M. V.; Lodge, T. P. *Macromolecules* **1992**, *25* (15), 3896–3901.

(2) Olsen, B. D.; Segalman, R. a. *Macromolecules* **2006**, *39* (20), 7078–7083.

(3) Boutris, C.; Chatzi, E. G.; Kiparissides, C. *Polymer (Guildf).* **1997**, *38* (10), 2567–2570.

(4) Pédelacq, J.-D.; Cabantous, S.; Tran, T.; Terwilliger, T. C.; Waldo, G. S. *Nat. Biotechnol.* **2006**, *24* (1), 79–88.

(5) Zhang, L.; Daniels, E. S.; Dimonie, V. L.; Klein, A. *J. Appl. Polym. Sci.* **2010**, *118*, 2502–2511.

(6) Haupts, U.; Maiti, S.; Schwille, P.; Webb, W. W. *Proc. Natl. Acad. Sci. U. S. A.* **1998**, *95* (November), 13573–13578.

(7) Lam, C. N.; Kim, M.; Thomas, C. S.; Chang, D.; Sanoja, G. E.; Okwara, C. U.; Olsen, B. D. *Biomacromolecules* **2014**, *15* (4), 1248–1258.

(8) Kozakov, D.; Beglov, D.; Bohnuud, T.; Mottarella, S. E.; Xia, B.; Hall, D. R.; Vajda, S. *Proteins Struct. Funct. Bioinforma.* **2013**, *81* (12), 2159–2166.

(9) Kozakov, D.; Brenke, R.; Comeau, S. R.; Vajda, S. *Proteins Struct. Funct. Bioinforma.* **2006**, *65*, 392–406.